Nonperturbative QCD treatment of high-energy hadron-hadron scattering

H.G. Dosch
Institut für Theoretische Physik der Universität Philosophenweg 16, D-69120 Heidelberg, Federal Republic of Germany

Erasmo Ferreira
Departamento de Física, Pontifícia Universidade Católica, Rio de Janeiro 22452 RJ, Brazil

A. Krämer
*SAP AG Systeme, D-69190 Walldorf, Federal Republic of Germany**
(Received 4 February 1994)

Total cross sections and logarithmic slopes of the elastic scattering cross sections for different hadronic processes are calculated in the framework of the model of the stochastic vacuum. The relevant parameters of this model, a correlation length and the gluon condensate, are determined from scattering data, and found to be in very good agreement with values coming from completely different sources of information. A parameter-free relation is given between total cross sections and slope parameters, which is shown to be remarkably valid up to the highest energies for which data exist.

PACS number(s): 12.38.Lg, 13.85.Dz, 13.85.Lg

I. INTRODUCTION

It is certainly a great challenge to establish a microscopic description of high-energy scattering in the framework of the field theory of strong interactions, i.e., QCD. Sophisticated treatments of perturbation theory [1] have lead to interesting results, which however are either qualitative or not able to explain the most striking phenomena. There is a rich amount of data on soft high-energy scattering, i.e., elastic scattering at high energies and momentum transfers smaller than the hadronic scale ($\approx$ 1 GeV). The newest and most precise data come from proton-antiproton scattering [2], extending up to center of mass energies $\sqrt{s} = 1800$ GeV. There are older data in the pp, πp, and Kp channels [3,4], and for other hadronic channels, such as the Σp system [5], they are still scarce. More soft-scattering data are expected for the near future from Fermilab and the CERN Large Hadronic Collider (LHC).

The energy dependence, in the full range of available data, is well described in the Regge picture [6] . The total cross sections [7] increase with energy like $s^{0.0808}$, leading to a hypercritical Pomeron intercept. The variation of the slope of the elastic scattering cross sections is also well described in the Regge picture with a slope of the Pomeron trajectory $\alpha'(t) = 0.25$ GeV^{-2}.

The value of about 2/3 for the ratio of πp to pp (or $\bar{p}p$) total cross sections, as well as certain factorization properties, are suggestive of an additive quark model [8], in which the main features of high-energy scattering can be described through quark-quark scattering amplitudes. On the other hand, there is also a remarkable flavor dependence of the cross sections, which decrease with the increasing number of strange quarks in the scattering channel. Such a feature is most naturally explained in models in which the cross sections depend on the sizes of the hadrons, which is also indicated by the dependence of the slopes of the elastic differential cross sections on the hadron sizes [9].

In this paper we evaluate elastic scattering amplitudes of hadrons in the framework of the model of the stochastic vacuum (MSV), originally developed in order to treat non-perturbative effects in low-energy hadron physics [10,11]. The model therefore deals with parameters of nonperturbative QCD that play an essential role both in hadron spectroscopy and in high-energy scattering. Our treatment is based rather on loop-loop than on quark-quark scattering. An important consequence is that the high-energy cross sections depend on the sizes of the hadrons, and this effect is due to the same mechanism that leads to confinement.

The paper is organized as follows. In Sec. II we give the theoretical foundations of our model. In Sec. II A we shortly recapitulate essential aspects of the analysis of soft high-energy scattering and in Sec. II B some important features of the model of the stochastic vacuum are explained. In Sec. III we apply the MSV to soft high-energy scattering and in Sec. IV we evaluate the formalism derived in Sec. III and find convenient numerical representations for the results. In Sec. V we discuss the choice of input parameters and compare our theoretical results with experiment. In Sec. VI we present concluding remarks. In the appendices we discuss some more technical points.

*Present address.

II. THEORETICAL BACKGROUND

A. Soft high-energy scattering in nonperturbative QCD

The first field theoretical approaches to soft high-energy scattering at small momentum transfer were attempted by Amati, Fubini, and Stanghelini [12] in the framework of the multi-peripheral model and by Gell-Mann, Goldberger, and Low in a massive vector-exchange theory [13]. Since the time when it became clear that QCD is the fundamental theory of the strong interactions, many efforts were made to explain the relevant features of soft high-energy scattering, either by assuming genuine nonperturbative effects [14] or by elaborate summation of perturbative contributions [1] .

The success of methods, applied primarily in hadron spectroscopy, taking into account nonperturbative contributions as gluon condensates [15] stimulated Landshoff and Nachtmann [16] to apply nonperturbative concepts also to soft high-energy scattering. In an Abelian model they related elastic high-energy scattering to the nontrivial structure of the QCD vacuum, requiring, besides the (static) gluon condensate, a finite correlation length for the slowly varying (nonperturbative) gluon fields in the vacuum. In their Abelian model, this correlation leads effectively to a nonperturbative gluon propagator. The main consequences of the model were the correct spin structure (vectorlike exchange) of soft elastic high-energy scattering and quark additivity. The latter holds only if the above-mentioned correlation length of the gluon fields is small compared with the hadron radius. The energy dependence of the total cross section comes out only approximately correct, namely as a constant, instead of the experimentally observed slow rise like $s^{0.0808}$. This model has been applied successfully also to other channels [17].

The structure of nonperturbative contributions to high-energy scattering was further investigated in a more general way by Nachtmann [18], who reduced the nonperturbative parts in soft high-energy hadron scattering to quark-quark (antiquark) scattering, justifying this reduction in certain kinematical regions through considerations in the femtouniverse. Through the use of the eikonal method, the high-energy scale was separated and the (nonperturbative) part of the quark-quark scattering amplitude that is due to exchange of states with the vacuum quantum numbers could be reduced to an expression with the structure

$$\langle q^{C'}(p_1)\ q^{D'}(p_2')|q^{C}(p_1)\ q^{D}(p_2)\rangle$$

$$\underset{s\to\infty}{\longrightarrow} \bar{u}(p_1')\ \gamma^{\mu}u(p_1)\ \bar{u}(p_2')\ \gamma_{\mu}u(p_2)\ J_{qq}(q^2)\ \delta_{C'C}\delta_{D'D}\ , \tag{1}$$

with small momentum transfer $q = p_1' - p_1 = p_2' - p_2$. The upper indices C, D denote the colors of the quarks, and $u(p)$ is a Dirac spinor.

The transition from the quark-quark scattering amplitude to the observable hadron-hadron scattering amplitude was achieved through current matrix elements occurring in deep inelastic scattering.

In this paper we widely follow the general analysis of Nachtmann [18], and evaluate quark-quark scattering amplitudes in a specific nonperturbative model, namely that of a stochastic vacuum with Gaussian fluctuations [10,11] of the field strength. There is however a very specific difference: whereas the original treatment of Nachtmann is based on a reduction of hadron-hadron scattering to quark-quark scattering, our basic entities are scattering amplitudes for Wilson loops in Minkowski space-time. A definite advantage of our approach is the gauge invariance of these amplitudes in contradistinction to the quark-quark amplitudes. The loop amplitudes treated here can also be obtained in the framework of Nachtmann [18], if one starts with hadron-hadron rather than with quark-quark scattering matrix elements (O. Nachtmann, private communication).

Another important difference must be remarked. Quark additivity appears in a natural way in the Landshoff-Nachtmann model [16] and in the extended framework of Nachtmann [18]. Here each quark interacts with the vacuum field, and we may consider that this interaction defines a region with the form of a tube around the quark path. Since the interaction with another quark is due to the correlations of the fields in two such tubes, the *effective* radius of a tube is actually determined by the correlation length of the vacuum field. The qq interactions occur only in the regions where two such tubes overlap. If the separation of the quarks inside a hadron is large compared with the correlation length a, the interaction regions for the different pairs of quarks when two hadrons collide are indeed well separated from each other, and quark additivity holds. However, such an argument is dangerous in a nonperturbative treatment, since, for instance, it would not lead to the area law for the Wilson loop. Indeed, it is well known that even a short range correlation of the fields can lead to long range effects due to potentials, since the step from the fields to the potentials is essentially nonlocal. A good example of this phenomenon is the Bohm-Aharonov effect [19], where the phase of an electron can be influenced by a magnetic field located far away. These long range effects might spoil quark additivity, and we show in Sec. II B that this is indeed the case with the model of the stochastic vacuum: the same effect which leads to confinement also leads to a violation of quark additivity. The physical reason for that is easy to understand, since not only the quarks but also the glue between them participate essentially in the scattering process. We return to this point in technical detail in Sec. II B.

B. The model of the stochastic vacuum

The model of the stochastic vacuum [10,11] is based on the idea that the low frequency contributions in the functional integral can be taken into account by a simple stochastic process with a converging cluster expansion [20]. This assumption leads, in a non-Abelian gauge theory, to linear confinement of static color sources.

Let us phrase this idea in a somewhat more formal

language. Let $\mathcal{D}\tilde{\phi}(k)\ e^{-S[\tilde{\phi}]}$ be the functional measure of a quantum field theory where the fields to be integrated over are expressed in momentum space. If the measure is split into low and high frequency parts,

$$\mathcal{D}\tilde{\phi}(k) = \prod_{|k|<\mu} \mathcal{D}\tilde{\phi}(k) \prod_{|k|>\mu} \mathcal{D}\tilde{\phi}(k) \ , \tag{2}$$

the integration over the high frequencies can be accounted for perturbatively, in an asymptotically free theory. All terms of higher than quadratic order in the fields occurring in the exponential of the action $e^{-S[\tilde{\phi}]}$ are expanded in a power series and, since only quadratic terms are kept in the exponent, the remaining functional integrals are Gaussian.

Little is known about the functional integration over the low frequencies. In the QCD sum rule approach [15], the contribution of this part is taken into account by power corrections proportional to specific nonperturbative vacuum expectation values (condensates). A model which goes further is that of the stochastic vacuum [10,11] in its most restrictive form. Since we know that nature has managed to regularize the infrared problems of perturbative theory (after all, we do observe hadrons), we may assume that the integration measure of the low frequency fields may be approximated by a simple functional measure. The simplest ansatz is that of a Gaussian integration measure, which is specified by a correlator (corresponding to the propagator in perturbation theory). This correlator is (apart from its specific form) determined by two scales: the strength of the correlator and the correlation length.

Generically, we may write

$$\int \prod_{|k|<\mu} \mathcal{D}\tilde{\phi}(k) e^{-S}\ \phi(x_1)\ \phi(x_2) \equiv \langle \phi(x_1)\phi(x_2)\rangle_A = G(x_1 - x_2) \ , \tag{3}$$

and obtain all other Green's functions for a Gaussian process by factorization. Note that we have liberally switched between the fields in coordinate space, $\phi(x)$, and in momentum space, $\tilde{\phi}(k)$. Equation (3) describes only the low internal frequencies part of the correlator, and thus $G(x_1 - x_2)$ is supposed to be regular for $x_1 \to x_2$. The singularities are due to perturbative terms. As mentioned above, this simple model leads to confinement in a non-Abelian gauge theory, and moreover the heavy quark potential deduced from the correlation determining the Gaussian stochastic process agrees very well with phenomenological determinations [21,22]. Thus it is not unreasonable to apply the approximation by a Gaussian process to other nonperturbative phenomena, as soft high-energy scattering.

First we discuss some basic properties of the two-point correlator defining the nonperturbative Gaussian process (i.e., the approximation for the measure of functional integration over the low frequency fields). As always occurs with approximations, a control of gauge invariance is essential. If that control is missing, one is never sure whether the output of the calculation is only a gauge artifact. So we do not deal with the correlator of the gauge potentials $A^F_\mu(x)$, but rather of the field strengths $F^F_{\mu\nu}$, where the upper index F is the color index of the adjoint representation. As usual, we introduce the Lie-algebra-valued field quantities

$$\mathbf{A}_\mu(x) = \sum_{F=1}^{N_c^2-1} A^F_\mu(x)\ \tau_F \ , \quad \mathbf{F}_{\mu\nu}(x) = \sum_{F=1}^{N_c^2-1} F^F_{\mu\nu}\ \tau_F \ , \tag{4}$$

and the covariant derivative

$$\mathbf{D}_\mu = \left(\mathbf{1}\frac{\partial}{\partial x_\mu} - ig\mathbf{A}_\mu\right) \ . \tag{5}$$

In the expression above, τ_F represents the $N_c^2 - 1$ generators of the Lie algebra of the gauge group $\mathrm{SU}(N_c)$. For $N_c = 3$ they are, in the fundamental representation, $1/2$ times the Gell-Mann matrices λ_F. If not stated otherwise, we always use the fundamental representation. For some later discussions [see Eq. (36) below], it is convenient to work with a general number of colors N_c. In the first part of this section we work, as usual in the functional approach, in a Euclidean space-time continuum, and therefore only lower Lorentz indices are used.

In a non-Abelian gauge theory the field strength tensor $\mathbf{F}_{\mu\nu}(x)$ does change under a local gauge transformation

$$\mathbf{F}_{\mu\nu}(x) \to \mathbf{U}(x)\ \mathbf{F}_{\mu\nu}(x)\ \mathbf{U}^{-1}(x) \ , \tag{6}$$

where $\mathbf{U}(x)$ is a local element of the gauge group $\mathrm{SU}(N_c)$.

In order to give a well-defined meaning to a correlator, which is a bilocal object, we parallel transport the color content of all fields to a single reference point w, i.e., we consider the parallel-transported field strength tensor

$$\mathbf{F}_{\mu\nu}(x;w) := \phi^{-1}(x,w)\ \mathbf{F}_{\mu\nu}(x)\ \phi(x,w) \ , \tag{7}$$

where $\phi(x,w)$ is a non-Abelian Schwinger string from point w to point x:

$$\phi(x,w) = \mathbf{P}\exp\left[-ig\int_0^1 d\sigma\ (x-w)_\mu \times \mathbf{A}_\mu[w + \sigma(x-w)]\right] . \tag{8}$$

$\mathbf{P}$ denotes path ordering, which is necessary in order to give to the exponential a well-defined meaning. In a nonperturbative way, this ordering is defined, for any operator $\mathcal{O}$ through

$$\mathbf{P}\exp\left[i\int_0^1 \mathcal{O}(\sigma)\ d\sigma\right] = \lim_{\Delta\sigma\to 0}\prod_k \exp\left[i\mathcal{O}\left(\frac{\sigma_k + \sigma_{k-1}}{2}\right)\Delta\sigma_k\right] \ , \tag{9}$$

with $0 < \sigma_1 < \sigma_2 \cdots < 1$, $\Delta\sigma_k = \sigma_{k+1} - \sigma_k$.

The field strength tensor in Eq. (7) transforms with

the gauge transformation at the fixed reference point w:

$$\mathbf{F}_{\mu\nu}(x,w) \to \mathbf{U}(w)\ \mathbf{F}_{\mu\nu}(x;w)\ \mathbf{U}^{-1}(w)\ . \tag{10}$$

The correlator $\langle \mathbf{F}_{\mu\nu}(x,w)\ \mathbf{F}_{\delta\sigma}(y,w)\rangle_A$, i.e., the vacuum expectation value with respect to the low frequencies, is gauge covariant because of Eq. (10); in general, it may depend on the two coordinate differences $(x-w)$ and $(y-w)$. We now make the crucial approximation that the correlator is independent of the reference point w, and thus only depends on the difference $z = x - y$. This approximation becomes exact for $x \to y$, and is nearly true for w fixed and large distances $z = x - y$. In this approximation, the most general form of the correlator [11] is given by

$$\begin{aligned}\left\langle g^2\ F^C_{\mu\nu}(x,w)\ F^D_{\rho\sigma}(y,w)\right\rangle_A &= \frac{\delta^{CD}}{N_c^2-1}\ \frac{1}{12}\langle g^2\ FF\rangle \\ &\times \cdot\left\{\kappa(\delta_{\mu\rho}\ \delta_{\nu\sigma} - \delta_{\mu\sigma}\ \delta_{\nu\rho})D(z^2/a^2)\right. \\ &\left.+(1-\kappa)\frac{1}{2}\left[\frac{\partial}{\partial z_\mu}(z_\rho\delta_{\nu\sigma} - z_\sigma\delta_{\nu\rho}) + \frac{\partial}{\partial z_\nu}(z_\sigma\delta_{\mu\rho} - z_\rho\delta_{\mu\sigma})\right]D_1(z^2/a^2)\right\}\ . \end{aligned}\tag{11}$$

Here $z = x - y$, a is a characteristic correlation length, $\langle g^2\ FF\rangle$ is the gluon condensate

$$\langle g^2\ FF\rangle = \langle g^2\ F^C_{\mu\nu}(0)\ F^C_{\mu\nu}(0)\rangle_A\ , \tag{12}$$

N_c is the number of colours, $C, D = 1, \ldots, N_c^2 - 1$, and the factors in Eq. (11) are chosen in such a way that

$$D(0) = D_1(0) = 1\ . \tag{13}$$

The two possible tensor structures are arranged in order that the second term satisfies the homogeneous Maxwell equation, i.e.,

$$\frac{\partial}{\partial x_\beta}\ \varepsilon_{\alpha\beta\mu\nu}\left\langle g^2\ F^C_{\mu\nu}(x,w)\ F^C_{\rho\sigma}(y,w)\right\rangle_A = 0 \quad \text{for } \kappa = 0\ . \tag{14}$$

Hence, in an Abelian gauge theory without monopoles, where the homogeneous Maxwell equations must hold, only the second structure can occur, i.e., we must there have $\kappa = 0$. However, in a non-Abelian theory there is no reason for κ to be zero.

With the form of Eq. (11) for the correlator, one obtains [10,11] the area law for a Wilson loop with the string tension ρ, given by

$$\rho = \frac{\kappa\pi}{144}\ \langle g^2\ FF\rangle a^2 \int_0^\infty D(-u^2)\ du^2\ . \tag{15}$$

Thus only the tensor structure proportional to D leads to confinement. This result has the very welcome consequence that only in non-Abelian gauge theories the model of the stochastic vacuum leads to confinement. It also teaches us that the correlator D is the part specific to non-Abelian gauge theories.

The correlator in Eq. (11) has been calculated on the lattice [23], and the results show unambiguously that κ is different from zero, as predicted by the model of the stochastic vacuum. The ratio $\kappa/(1-\kappa)$ is rather large (about 3), so that $D(z^2/a^2)$ is the dominant contribution. We return to this point in more detail later.

III. THE MODEL OF THE STOCHASTIC VACUUM IN HIGH-ENERGY SCATTERING

The correlator in Eq. (11), specifying the Gaussian process that approximates non-perturbative effects of QCD, is the starting point for our evaluation of observables in soft high-energy scattering. In the analysis mentioned in Sec. II, Nachtmann [18] evaluated the quark-quark scattering amplitude using the eikonal approximation for the interaction of the quarks with the gluon field. In a first step, we follow the same approach, and consider the scattering amplitude of a single quark in a given external color potential $\mathbf{A}_\mu$. If the energy of the quark is very high and the background field has only a limited frequency range, the quark moves on an approximately straight lightlike line and the eikonal approximation can be applied. At the end of this section we recall the condition for the validity of the eikonal approximation.

Along its path Γ, the quark picks up the eikonal phase (which is here a unitary $N_c \times N_c$ matrix)

$$V = \mathbf{P}\exp\left(-ig\int_\Gamma \mathbf{A}_\mu(z)\ dz^\mu\right)\ . \tag{16}$$

Here $\mathbf{A}_\mu$ is again the Lie-algebra-valued potential and $\mathbf{P}$ denotes path ordering [see Eq. (9)]. The phase factor for an antiquark is obtained by complex conjugation.

From the scattering amplitudes for single quarks in the background field, we obtain the nonperturbative quark-quark scattering amplitude by functional integration over the background field of the product of the two scattering amplitudes. More specifically, consider two quarks traveling along the lightlike paths Γ_1 and Γ_2 given by

$$\Gamma_1 = (x^0, \vec{b}/2, x^3 = x^0)$$

and (17)

$$\Gamma_2 = (x^0, -\vec{b}/2, x^3 = -x^0)\ ,$$

corresponding to quarks moving with velocity of light

in opposite directions, with an impact vector $\vec{b}$ in the x^1x^2 plane (referred to in the following as the transverse plane). Let $V_{1,2}(\pm\vec{b}/2)$ be the phases picked up by the quarks along these paths

$$V_{1,2}(\pm\vec{b}/2) = \mathbf{P}\exp\left[-ig\int_{\Gamma_{1,2}} \mathbf{A}_\mu(z)\, dz^\mu\right] . \quad (18)$$

Then the scattering amplitude for two quarks with momenta p_1, p_2 and color indices c_1, c_2 leading to two quarks of momenta p_3, p_4 and colors c_3 c_4 is given by [18]

$$T_{c_3c_4;c_1c_2}(s,t) = \bar{u}(p_3)\,\gamma^\mu(p_1)\,\bar{u}(p_2)\,\gamma_\mu u(p_2)\,\mathcal{V} , \quad (19)$$

where

$$\mathcal{V} = i\langle Z_\psi^{-2}\rangle_A\left\langle \int d^2\vec{b}\; e^{-i\vec{q}\cdot\vec{b}}\left\{\left[V_1\Big(-\frac{\vec{b}}{2}\Big)-1\right]_{c_3c_1}\times\left[V_2\Big(+\frac{\vec{b}}{2}\Big)-1\right]_{c_4c_2}\right\}\right\rangle_A . \quad (20)$$

Here $\langle\ \rangle_A$ denotes functional integration over the background field; $\vec{q}$ is the momentum transfer (p_1-p_3) projected on the transverse plane. Of course the approximation makes sense only if $|\vec{q}| \ll |\vec{p}|$. The quantity Z_ψ is the fermion wave-function renormalization constant in the eikonal approximation, given by [18]

$$Z_\psi[A] = \frac{1}{N_c}\mathrm{tr}\,[V_1(0)] = \frac{1}{N_c}\mathrm{tr}\,[V_2(0)] . \quad (21)$$

The subtraction of the unit operator from the phase matrices V is due to the transition from the S to the T operator.

In the limit of high energies we have helicity conservation

$$\bar{u}(p_3)\,\gamma^\mu u(p_1)\,\bar{u}(p_4)\,\gamma_\mu u(p_2) \underset{s\to\infty}{\longrightarrow} 2s\delta_{\lambda_1\lambda_3}\delta_{\lambda_4\lambda_2} , \quad (22)$$

where λ_i are the helicities of the quarks and $s = (p_1+p_2)^2$. In the following we can thus ignore the spin degrees of freedom.

The scattering amplitude in Eq. (19) is explicitly gauge dependent and the cautioning remarks made in the last section apply here. But we know that, in meson-meson scattering, for each quark there is an antiquark moving on a nearly parallel line. Furthermore, the meson must be a color singlet state under local gauge transformations. To construct such a colorless state we have to parallel transport the color content from the quark to the antiquark (or vice versa) in the same way as discussed in Sec. II for the field-strength tensor. Since this parallel transport of the colors is made by a Schwinger string $\phi(x_q, x_{\bar{q}})$ [see Eq. (8)], we obtain for the meson a Wilson loop whose lightlike sides are formed by the quark and antiquark paths, and front ends by the Schwinger strings (see Fig. 1). The direction of the path of an antiquark is effectively the opposite of that of a quark, so that the loop has a well-defined internal direction. The resulting loop-loop amplitude is now specified, not only by the impact parameter, but also by the transverse extension vectors.

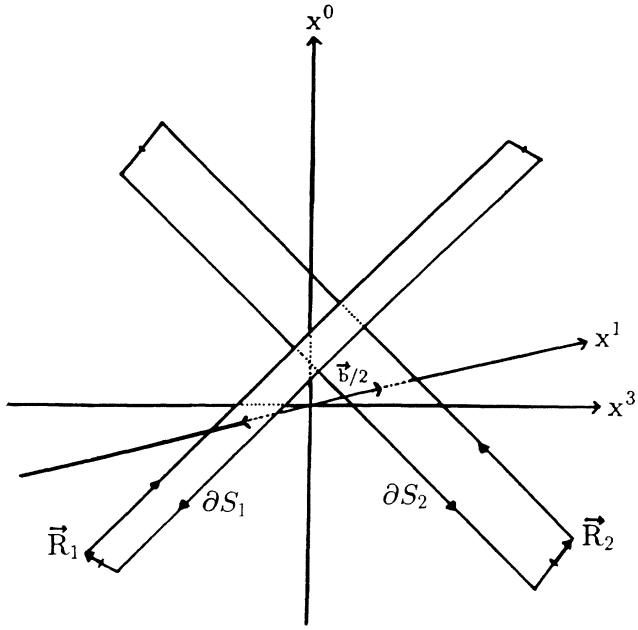

FIG. 1. Wilson loops formed by the paths of quarks and antiquarks inside two mesons. The impact vector $\vec{b}$ is the distance vector between the middle lines of the two loops. $\vec{R}_1$ and $\vec{R}_2$ are the vectors in the transverse plane from the middle lines to the quark lines of meson 1 and 2, respectively. For the antiquarks the corresponding vectors are $-\vec{R}_1$ and $-\vec{R}_2$. The front lines of the loops guarantee that the mesons behave as singlets under local gauge transformations.

We thus introduce the loop-loop scattering amplitude

$$J(\vec{b},\vec{R}_1,\vec{R}_2) = \left[\left\langle\frac{1}{N_c}\mathrm{tr}\,W_1(0,\vec{R}_1)\right\rangle_A\left\langle\frac{1}{N_c}\mathrm{tr}\,W_2(0,\vec{R}_2)\right\rangle_A\right]^{-1} \times\left\langle\frac{1}{N_c}\mathrm{tr}\left[W_2\Big(-\frac{\vec{b}}{2},\vec{R}_2\Big)-1\right]\frac{1}{N_c}\mathrm{tr}\left[W_1\Big(-\frac{\vec{b}}{2},\vec{R}_1\Big)-1\right]\right\rangle_A , \quad (23)$$

where $W_1(-\vec{b}/2,\vec{R}_1)$ is the Wilson loop

$$W_1\left(-\frac{\vec{b}}{2},\vec{R}_1\right) = \mathbf{P}\exp\left[-ig\oint_{\partial S_1}\mathbf{A}_\mu(z)\,dz^\mu\right] . \quad (24)$$

The closed loop ∂S_1 is a rectangle whose long sides are formed by the quark path $\Gamma_1^q = (x_0, \vec{b}/2+\vec{R}_1, x_3 = x_0)$ and the antiquark path $\Gamma_1^{\bar{q}} = (x_0, \vec{b}/2-\vec{R}_1, x_3 = x_0)$ and whose front sides are formed by lines from $(T, \vec{b}/2+$

$\vec{R}_1, T)$ to $(T, \vec{b}/2 - \vec{R}_1, T)$ for large positive and negative T (we will then take the limit $T \to \infty$). $W_2(\vec{b}/2, \vec{R}_2)$ is constructed analogously. The first factor in Eq. (23) is the loop renormalization constant that replaces the quark field renormalization in Eq. (20).

Our next aim is to perform the functional integration over A by applying the model of the stochastic vacuum discussed in the preceding section. Since the correlator is given in terms of the parallel-transported field tensor $\mathbf{F}_{\mu\nu}(x, w)$, we have first to transform the line integrals $\int \mathbf{A}_\mu dz^\mu$ through integrals over the field tensor. This is done with the help of the non-Abelian Stokes theorem [24]. By deforming the path as indicated in Fig. 2, we can express the line integral $\oint_{\partial S} \mathbf{A}_\mu(z)\, dz^\mu$, where the closed path ∂S goes from w to $x_{(1)}$ then to $x_{(2)}$ and back to w, into the surface integral $\int_S \mathbf{F}_{\mu\nu}(z, w)\, d\Sigma^{\mu\nu}(z)$, where $d\Sigma^{\mu\nu}(z)$, with $\mu < \nu$, is the element of the surface S at point z. Here we have used that, for a sufficiently small contour, we have

$$\oint_{\partial S} \mathbf{A}_\mu dz^\mu = \int_S \mathbf{F}_{\mu\nu} d\Sigma^{\mu\nu} + O(S^2) \ . \tag{25}$$

In this way we obtain

$$\mathbf{P} \exp \int_{\partial S} -ig\mathbf{A}_\mu(z)\, dz^\mu = \mathbf{P}_S \exp \int_S -ig\mathbf{F}_{\mu\nu}(z, w) \times d\Sigma^{\mu\nu}(z) \ , \tag{26}$$

where $\mathbf{P}_S$ now denotes surface ordering according to Fig. 2. Since the reference point w in the correlator (11) must be the same for both fields, we have to choose a common reference point for both traces in the product

$$\left\langle \mathrm{tr} \left[W_1\Big(-\frac{\vec{b}}{2}, \vec{R}_1\Big) - 1 \right] \mathrm{tr} \left[W_2\Big(\frac{\vec{b}}{2}, \vec{R}_2\Big) - 1 \right] \right\rangle_A \ . \tag{27}$$

We choose the point w in the most symmetric way and then the surface emerging from the loop ∂S_1 is formed by the sliding sides of a pyramid with the loop ∂S_1 as basis and the point with coordinates w as apex; the same holds for ∂S_2 (see Fig. 3).

Before its application to high-energy scattering, the model of the stochastic vacuum must be translated from Euclidean space-time, in which it is naturally formulated, to the Minkowski continuum. Unfortunately we cannot go the other way and continue Eq. (23) to the Euclidean continuum, which would be the safe way from the point of view of the functional integration. However the Wilson loops occurring in Eq. (23) have lightlike sides which would shrink to a point if continued to a space time continuum with Euclidean metric. We think that this is a serious obstacle in all attempts to evaluate soft high-energy amplitudes numerically on a lattice.

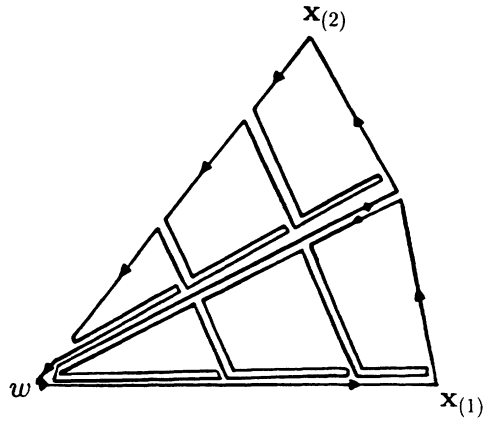

FIG. 2. Representation of the non-Abelian Stokes theorem. The contour integral running from w to $x_{(1)}$ then to $x_{(2)}$ and back to w is deformed in order to become a surface integral. Here $x_{(1)}$ and $x_{(2)}$ represent the coordinates of the quark and antiquark in a meson, respectively.

Since we cannot adapt the scattering amplitude to the Euclidean world, we have to proceed the other way and adapt the model of the stochastic vacuum to the Minkowski world. We are fully aware that this is by no means a trivial step and, pending a better analytical understanding of nonperturbative effects, we have to let the experiment decide on the justification. (Similar problems occur when one applies instanton effects to high-energy scattering [25].) Thus we must translate the correlation function in Eq. (11) to the Minkowski world. This is obvious for the tensor structure, where we just substitute $\delta_{\mu\nu}$ by $-g_{\mu\nu}$, etc., but simple choices for the correlation functions like $\exp(-z^2/a^2)$ or $\exp(-\sqrt{z^2}/a)$ cannot be analytically continued in a meaningful way. Therefore, we must look for correlation functions $D(z^2/a^2)$ and $D_1(z^2/a^2)$ that fall off for negative z^2 values (corresponding to Euclidean distances), and whose Fourier transforms exist in Minkowski metric, since these will enter essentially in the scattering amplitudes. An ansatz for the correlator that fulfills this requirement can be written in terms of the Fourier transforms

$$\langle g^2\, F^C_{\mu\nu}(x, w)\, F^D_{\rho\sigma}(y, w)\rangle_A = \frac{\delta^{CD}}{N_c^2 - 1} \frac{1}{12} \langle g^2 FF\rangle \int \frac{d^4k}{(2\pi)^4}\, e^{-ik(x-y)/a} \Big\{ (g_{\mu\rho}g_{\nu\sigma} - g_{\mu\sigma}g_{\nu\rho})\, \kappa i\widetilde{D}(k^2) + (-g_{\nu\sigma}k_\mu k_\rho + g_{\nu\rho}k_\mu k_\sigma - g_{\mu\rho}k_\nu k_\sigma + g_{\mu\sigma}k_\nu k_\rho)(1 - \kappa)\, i\frac{d\widetilde{D}_1(k^2)}{dk^2} \Big\} \ , \tag{28}$$

where

$$i\widetilde{D}(k^2) = \int d^4z D(z^2/a^2)\, e^{ikz/a} \tag{29}$$

and

$$i\widetilde{D}_1(k^2) = \int d^4z D_1(z^2/a^2)\, e^{ikz/a} \ . \tag{30}$$

After this choice is made, all functional integrations can be performed, in principle. The quantities $W_{1,2}$ in Eqs. (23) and (24) can be expressed as surface integrals,

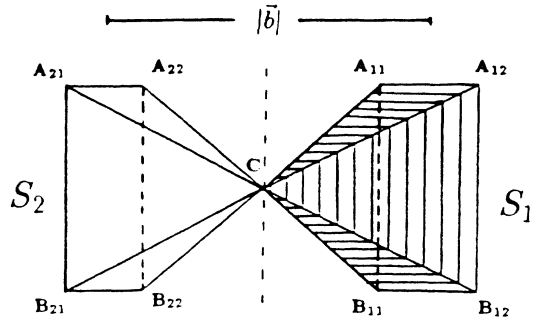

FIG. 3. Tilted perspective view of the surfaces S_1 and S_2 obtained from the line integrals along the Wilson loops ∂S_1 and ∂S_2 after appying the non-Abelian Stokes theorem. The line $\overline{B_{i1}A_{i1}}$ is the quark path line and $\overline{B_{i2}A_{i2}}$ is the antiquark path line of meson i. C is the reference point (with coordinates w in the non-Abelian Stokes theorem).

according to Eq. (26). The exponential being expanded, the expectation value can be calculated using Eq. (26) and assuming factorization in a Gaussian process (see below).

Before we enter into details, we make two remarks which facilitate further calculations. First we note that, since

$$\langle \mathrm{tr} W_1 \rangle_A = \langle \mathrm{tr} W_2 \rangle_A = N_c \ , \tag{31}$$

the functional integral over the surface of one pyramid alone vanishes. To see the formal reason for Eq. (31), we remark that in the evaluation of a single loop, say $\langle \mathrm{tr} W_1 \rangle_A$, only the expectation value $\langle e_+^\mu F_{\mu i}(x,w) e_+^\rho F_{\rho k}(y,w) \rangle_A$ occurs, where e_+^μ is the lightlike vector $(1,0,0,-1)$, and i,k (1 or 2) are indices of the transverse plane. These correlators are zero by virtue of the tensor structures given in Eq. (28) (note that $e_+^\mu e_{+\mu} = 0$). Therefore only the unit term contributes, leading to Eq. (31). This is not in contradiction to the area law in Euclidean space-time, since the area of loops with lightlike sides would be zero in Euclidean metric.

Due to this mechanism, the quantities

$$Z_\psi = \left\langle \frac{1}{N_c} \mathrm{tr} W_1(0, \vec{\mathrm{R}}_i) \right\rangle_A \tag{32}$$

that enter in the first factor of the expression in Eq. (23) are equal to one (no loop renormalization). In the same way only mixed terms, from different pyramids, contribute for the expectation value in Eq. (23), since the correlation functions arising from the expansion of $\mathrm{tr} W_1(-\vec{\mathrm{b}}/2, \vec{\mathrm{R}}_1)$ alone, or equivalently of $\mathrm{tr} W_2(\vec{\mathrm{b}}/2, \vec{\mathrm{R}}_2)$, contain only field projections $e_-^\mu F_{\mu i}$ or $e_+^\mu F_{\mu i}$, respectively.

We next expand the exponentials W_i in Eq. (23). Since in the expansion of the trace of the exponential at least two terms are necessary ($\mathrm{tr}\tau_A = 0$), and because of Eq. (31) the lowest-order contribution to the loop-loop scattering amplitude is given by

$$J(\vec{\mathrm{b}}, \vec{\mathrm{R}}_1, \vec{\mathrm{R}}_2) = -(-ig)^4 \left(\frac{1}{2!}\right)^2 \mathrm{tr}\,[\tau_{C_1}\tau_{C_2}]\ \mathrm{tr}\,[\tau_{D_1}\tau_{D_2}] \cdot \int_{S_1} \prod_{i=1}^{2} d\Sigma^{\mu_i\nu_i}(x_i) \int_{S_2} \prod_{j=1}^{2} d\Sigma^{\rho_j\sigma_j}(y_j)$$
$$\times \frac{1}{N_c^2} \left\langle F^{C_1}_{\mu_1\nu_1}(x_1,w)\ F^{C_2}_{\mu_2\nu_2}(x_2,w)\ F^{D_1}_{\rho_1\sigma_1}(y_1,w)\ F^{D_2}_{\rho_2\sigma_2}(y_2,w) \right\rangle_A + \text{higher correlators} \ . \tag{33}$$

We next apply the factorization hypothesis

$$\langle F^{C_1} F^{C_2} F^{D_1} F^{D_2} \rangle = \langle F^{C_1} F^{C_2} \rangle \langle F^{D_1} F^{D_2} \rangle + \langle F^{C_1} F^{D_1} \rangle \langle F^{C_2} F^{D_2} \rangle + \langle F^{C_1} F^{D_2} \rangle \langle F^{C_2} F^{D_1} \rangle \ , \tag{34}$$

where the arguments and the Lorentz indices of F^{C_i}, F^{D_i} are the same as in Eq. (33).

We have checked that the higher-order terms are indeed small as compared to the leading term, and therefore we neglect them in the following. In this way the surface ordering indicated in Eq. (26) becomes irrelevant.

It is convenient to introduce the eikonal function χ:

$$\chi(\vec{\mathrm{b}}, \vec{\mathrm{R}}_1, \vec{\mathrm{R}}_2) = (-ig)^2 \int_{S_1} d\Sigma^{\rho\mu}(x) \int_{S_2} d\Sigma^{\sigma\nu}(y)$$
$$\times \langle F^C_{\rho\mu}(x,w)\ F^C_{\sigma\nu}(y,w) \rangle_A \ . \tag{35}$$

Then the loop-loop amplitude $J(\vec{\mathrm{b}}, \vec{\mathrm{R}}_1, \vec{\mathrm{R}}_2)$ is given to the lowest order in the correlator by

$$J(\vec{\mathrm{b}}, \vec{\mathrm{R}}_1, \vec{\mathrm{R}}_2) = -\frac{1}{N_c^2} \frac{1}{8} \frac{1}{(N_c^2-1)} \left[\chi(\vec{\mathrm{b}}, \vec{\mathrm{R}}_1, \vec{\mathrm{R}}_2) \right]^2 \ . \tag{36}$$

We notice the presence of the color suppression factor $1/(N_c^2-1)$ that always occurs in interactions between colorless objects. The eikonal function is determined by the geometry and by the correlator (28).

For the Fourier transform $\widetilde{D}(k^2)$ of the scalar correlation function D, that enters in Eq. (28), we introduce an ansatz which fulfills the requirements made above, and write

$$\widetilde{D}(k^2) = \frac{-6iA_n k^2}{(k^2 - 1/\lambda_n^2)^n} \frac{1}{\lambda_n^{2n-6}}, \ n \geq 4 \ , \tag{37}$$

with

$$D(z^2/a^2) = \int \widetilde{D}(k^2)\ e^{-ikz/a} \frac{d^4k}{(2\pi)^4} \ . \tag{38}$$

These functions are discussed in Appendix A. The constants A_n and λ_n are fixed by the normalization conditions

$$D(0) = 1 \text{ and } \int_0^\infty du D(-u^2) = 1 \ . \tag{39}$$

The second of these conditions allows the identification of a as a correlation length.

The string tension for the correlator of the form (37) can be obtained [11] from Eq. (15). With our choice for the correlator, we have [26]

$$\rho = \kappa \langle g^2 \ FF \rangle a^2 \frac{2}{81}(n-3)\left[\frac{\Gamma(n-3)}{\Gamma(n-5/2)}\right]^2 \ . \tag{40}$$

The scalar function D_1 is completely independent from D, and may have different values for the parameters a and n. Lattice calculations [23] show however that the forms of D and D_1 in the Euclidean region at large distances are similar, with D about three times larger than D_1. We show in Appendix B that even with equal weights for the two functions, the contribution of D to high-energy soft scattering is by far the dominant one, so that we can safely concentrate on this function.

Since analytic calculations are most easily done for the case $n \to \infty$, previous calculations have been made with that choice [26–29], but for $n = 4$ there is good agreement with the form (exponentially decreasing at large distances) indicated by lattice calculations in the Euclidean region [23]; we therefore adopt this form in the present work.

Up to now we have only considered loop-loop scattering amplitudes. It would be highly desirable to have a formalism relating these fundamental field theoretical entities to observables, corresponding to the operator product expansion for quark (and gluon) amplitudes. In the absence of such a formalism, we have to rely on a rather simple-minded quark model.

In a relativistic quark model, the distribution of the quarks is described by the transverse momentum $k_\perp$ and the fraction x of the longitudinal momentum carried by the quark. Since our amplitude is independent of the momentum of the quarks (as long as the energy is high enough to ensure lightlike paths), we may neglect the dependence on x, and only consider the transverse dependence. This transverse dependence is given by the Fourier transform of the transverse wave function, which determines the width $2|\vec{\mathrm{R}}|$ of the Wilson loops. We thus obtain our hadron-hadron (here still meson-meson) scattering amplitude by smearing over the values of $\vec{\mathrm{R}}_1$ and $\vec{\mathrm{R}}_2$ in Eq. (33) with transverse wave functions $\psi(\vec{\mathrm{R}})$. This leads to the meson-meson scattering amplitude

$$J_{MM'}(\vec{\mathrm{b}}) = \int d^2\vec{\mathrm{R}}_1 \int d^2\vec{\mathrm{R}}_2 \ J(\vec{\mathrm{b}}, \vec{\mathrm{R}}_1, \vec{\mathrm{R}}_2) \ |\psi_M(\vec{\mathrm{R}}_1)|^2 \times |\psi_{M'}(\vec{\mathrm{R}}_2)|^2 \ . \tag{41}$$

The choice of the transverse wave functions $\psi_M(\vec{\mathrm{R}})$ will be discussed in the next section.

For the treatment of the baryons we restrict ourselves to $N_c = 3$. We adopt two pictures: a genuine three-body configuration, and a diquark picture. In the latter the baryon is described exactly as a meson, where the diquark replaces the antiquark. In the three-body picture the baryon is described as shown in Fig. 4. There are three quark paths leading from $x_{(i)}$ to $x'_{(i)}$, $i = 1, 3$. The coordinates x_h and x'_h refer to the central point of the baryon. The paths from x_h to $x_{(i)}$ and x'_h to $x'_{(i)}$, respectively, must ensure that the baryon is a color singlet under local gauge transformations. This is done by parallel transporting the color from the quark positions $x_{(i)}$ to x_h, and coupling the colors antisymmetrically in the form

$$\frac{1}{\sqrt{6}} \varepsilon_{abc} \ \phi_{aa'}(x_h, x_{(1)}) \ \phi_{bb'}(x_h, x_{(2)}) \ \phi_{cc'}(x_h, x_{(3)}) \ , \tag{42}$$

where ϕ's are the Schwinger strings, Eq. (8). An analogous factor occurs at the end (primed coordinates), so that the baryon is described by the product of paths

$$\frac{1}{6} \varepsilon_{abc} \ \phi_{ad}[\Gamma_1] \ \phi_{be}[\Gamma_2] \ \phi_{cf}[\Gamma_3] \ \varepsilon_{def} \ , \tag{43}$$

where the path Γ_i leads from x_h over $x_{(i)}$ and $x'_{(i)}$ to x'_h. Let Γ_0 be the path leading from x'_h to x_h. Since $\phi[\Gamma_0] \in \mathrm{SU}(3)$, we have

$$\varepsilon_{def} = \varepsilon_{a'b'c'} \ \phi_{da'}[\Gamma_0] \ \phi_{eb'}[\Gamma_0] \ \phi_{fc'}[\Gamma_0] \ . \tag{44}$$

Inserting this expression into Eq. (43), we obtain that the baryon is represented by the product of Wilson loops (without traces)

$$\frac{1}{6} \varepsilon_{abc} W_{aa'}[\partial S_1] \ W_{bb'}[\partial S_2] \ W_{cc'}[\partial S_3] \ \varepsilon_{a'b'c'} \ , \tag{45}$$

where $W_{aa'}[\delta S_1] = \phi_{ad}[\Gamma_1] \ \phi_{da'}[\Gamma_0]$ is the loop from x_h to x_1, x'_1, x'_h and back to x_h. Thus for a baryon the factor $(1/N_c)\mathrm{tr}\ [W_1(-\vec{\mathrm{b}}/2, \vec{\mathrm{R}}_1) - \mathbf{1}]$ in Eq. (23) has to be replaced by

$$\frac{1}{36} \varepsilon_{abc} \varepsilon_{a'b'c'} \{ W_{a'a}(-\vec{\mathrm{b}}/2, \vec{\mathrm{R}}_1) \ W_{b'b}(-\vec{\mathrm{b}}/2, \vec{\mathrm{R}}_2) \ W_{c'c}(-\vec{\mathrm{b}}/2, \vec{\mathrm{R}}_3) - \delta_{aa'} \ \delta_{bb'} \ \delta_{cc'} \} \ . \tag{46}$$

Here $\vec{\mathrm{R}}_i$ is the vector extending from the middle line Γ_0 to the border of loop i. The impact parameter vector $\vec{\mathrm{b}}$ is taken with respect to the middle line Γ_0. The factor $1/36$ is due to color normalization. We discuss baryon transverse wave functions in the next section.

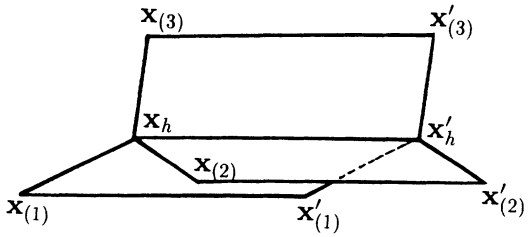

FIG. 4. Wilson loops (without traces) describing a baryon path in the three-body picture. The line from $x_{(i)}$ to $x'_{(i)}$ represents the path for the quark labelled i. The line from x_h to x'_h is the path for the central point of the baryon.

We conclude this section with some considerations concerning the validity of the underlying quark model, reviewing the analysis made by Nachtmann [18], who discusses limits on the energy values $\sqrt{s}$ in order to ensure the validity of his treatment. It is clear that the eikonal approximation can be justified only for a sufficiently high energy. A detailed analysis yields the condition $\sqrt{s} \geq 2\tau_0 h^{-2}$ where h is a typical hadronic scale ($h \sim 1$ GeV^{-1}) and τ_0 is the observation time of the scattering process in the *femtouniverse*. There is another scale Q_0 that indicates the separation between the perturbative and the nonperturbative effects. The correlation length and the wave function depend on its value, since it can be viewed as a renormalization scale for nonperturbative quantities. The value of Q_0 should also be approximately equal to the hadronic scale h^{-1}, and its relation with the energy and the observation time was found [18] to be

$$Q_0^2 \approx \frac{\sqrt{s}}{2\tau_0} \ . \tag{47}$$

From this relation Nachtmann also obtained a conservative *upper* bound for the energy, which results from the requirement that the observation time should be short enough so that the string between the scattering quarks or antiquarks is not broken if the two particles fly apart. The string breaks if the two quarks become so far apart that the potential energy of the string reaches the *protohadron* mass $m_c \approx 1.3$ GeV. Then the breaking time $\tau_{\rm cr}$ is determined by

$$\tau_{\rm cr} = \frac{m_c}{\rho} \ , \tag{48}$$

where ρ is the string tension $\rho \approx 0.18$ GeV^{-2} . The maximal observation time is given by $\tau_0 = 2\tau_{\rm cr}$. In the present paper we consider only elastic scattering of loops, where no string between quarks of different hadrons is formed, hence we see no compelling reason to apply the above limit to τ_0, and there is no upper limit on the energy for the applicability of the model from this consideration. However, for definiteness, we take in the present work as a reference energy the value $\sqrt{s} = 20$ GeV, corresponding to the conservative upper bound indicated by Nachtmann [18], and discuss other energies separately.

IV. NUMERICAL EVALUATION AND PARAMETRIZATION OF THE RESULTS

We now introduce the notation $\vec{\rm R}(I, L)$, where the first index (I=1,2) specifies the hadron, and the second specifies the particular quark or antiquark in that hadron. We first evaluate the eikonal functions $\chi(\vec{\rm b}, \vec{\rm R}(1,1), \vec{\rm R}(2,1))$ in Eq. (35) for the confining case, namely $\kappa = 1$. The integration surfaces S_1 and S_2 of the eikonal function

$$\chi(1\vec{\rm b}, \vec{\rm R}(1,1), \vec{\rm R}(2,1)) = (-ig)^2 \int_{S_1} d\Sigma^{\mu\nu}(x) \int_{S_2} d\Sigma^{\rho\sigma}(x') \times \langle F^C_{\mu\nu}(x,w) F^C_{\rho\sigma}(x',w) \rangle_A \tag{49}$$

are represented in Figs. 3 and 5. The first of these figures gives a somewhat tilted three-dimensional view, while the second shows a projection on the transverse plane. The vectors $\vec{\rm Q}(K, L)$ in the transverse plane connect the reference point C (with coordinates w) to the positions of the quarks and antiquarks of the loops 1 and 2. The quantity $\psi(K, L)$ is the angle between $\vec{\rm Q}(1, K)$ and $\vec{\rm Q}(2, L)$.

In the integrations indicated in Eq. (49) we first note that the contributions involving front planes ($CA_{11}A_{12}$, $CB_{11}B_{12}$, $CA_{21}A_{22}$, and $CB_{21}B_{22}$) in Fig. 3 vanish in the limit $T \to \infty$, and therefore we are left with four remaining terms, the integrals over the products of the side planes of two different pyramids. The four-dimensional integration over the two surfaces can be finally reduced to a single integration [26]. The integrations along the directions x_+ and x_- can be performed, and result in expressions involving two-dimensional inverse Fourier transforms of the correlator $\widetilde{D}(k^2)$. A typical resulting contribution that comes from the product of surfaces ($CA_{11}B_{11}$) and ($CA_{21}B_{21}$) in Fig. 3 is

$$\int_0^1 d\alpha \int_0^1 d\beta \, \cos\Psi(1,1) \, \mathcal{F}_2^{(4)}(-|\alpha\vec{\rm Q}(1,1) - \beta\vec{\rm Q}(2,1)|^2) \ , \tag{50}$$

where $\mathcal{F}_2^{(4)}$ is the above-mentioned two-dimensional Fourier transform of the correlator with $n = 4$ [see Eq. (37)], defined as

$$\mathcal{F}_2^{(4)}(-|\vec{\xi}|^2) = -\frac{1}{(2\pi)^2} \int d^2\vec{\rm K}_\perp \, \frac{6A_4\lambda_4^6 |\vec{\rm K}_\perp|^2}{(-\lambda_4^2|\vec{\rm K}_\perp|^2 - 1)^4} \times \exp(i\vec{\rm K}_\perp \cdot \vec{\xi}) \ , \tag{51}$$

where $\vec{\xi}$ is a two-dimensional vector of the transverse plane. This quantity, which is evaluated in Appendix A, can be can be written in the convenient form

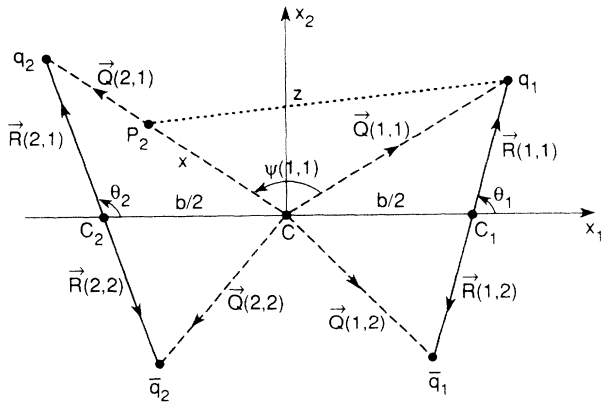

FIG. 5. Geometrical variables of the transverse plane, which enter in the calculation of the eikonal function for meson-meson scattering. The points C_1 and C_2 are the meson centers. In the integration, P_2 runs along the vector $\vec{\rm Q}(2,1)$, changing the length z, which is the argument of the correlator characteristic function. In analogous terms, points P_1, $\bar{P}_1$, and $\bar{P}_2$ run along $\vec{\rm Q}(1,1)$, $\vec{\rm Q}(1,2)$ and $\vec{\rm Q}(2,2)$. This explains the four terms that appear in Eq. (56).

$$\mathcal{F}_2^{(4)}(-|\vec{\xi}|^2) = -\frac{32}{9\pi}\Delta_2[(\rho|\vec{\xi}|)^3 K_3(\rho|\vec{\xi}|)] \ , \tag{52}$$

where

$$\rho = \frac{3\pi}{8} \ , \tag{53}$$

K_3 is a modified Bessel function, and Δ_2 is the Laplacian in two dimensions.

Taking advantage of the Laplacian form, we can apply Gauss' theorem in two dimensions and eliminate one further integration [26].

It is useful to introduce a reduced eikonal function and a reduced loop-loop scattering amplitude through

$$\widetilde{\chi}(\vec{b},\vec{R}_1,\vec{R}_2) \equiv \frac{12}{\kappa\langle g^2 FF\rangle}\chi(\vec{b},\vec{R}_1,\vec{R}_2) \tag{54}$$

and

$$\widetilde{J}_{MM'}(\vec{b},\vec{R}_1,\vec{R}_2) \equiv \frac{1}{\left[\kappa\langle g^2 FF\rangle\right]^2} J_{MM'}(\vec{b},\vec{R}_1,\vec{R}_2)$$
$$= -\frac{[\widetilde{\chi}(\vec{b},\vec{R}_1,\vec{R}_2)]^2}{144\times 8\times N_c^2(N_c^2-1)} \ . \tag{55}$$

[see Eq. (36)]. We then obtain

$$\widetilde{\chi}(\vec{b},\vec{R}(1,1),\vec{R}(2,1)) = -\cos\psi(1,1)\ I[Q(1,1),Q(2,1),\psi(1,1)] - \cos\psi(2,2)\ I[Q(1,2),Q(2,2),\psi(2,2)]$$
$$+\cos\psi(1,2)\ I[Q(1,1),Q(2,2),\psi(1,2)] + \cos\psi(2,1)\ I[Q(1,2),Q(2,1),\psi(2,1)] \ , \tag{56}$$

where the quantities I are given by

$$I[Q(1,K),Q(2,L),\psi(K,L)] = \frac{32}{9\pi}\left(\frac{3\pi}{8}\right)^2\left(Q(1,K)\int_0^{Q(2,L)}[Q(1,K)^2+x^2-2xQ(1,K)\cos\psi(K,L)]\right.$$
$$\times K_2\left[\frac{3\pi}{8}\sqrt{Q(1,K)^2+x^2-2xQ(1,K)\cos\psi(K,L)}\right]dx$$
$$+Q(2,L)\int_0^{Q(1,K)}[Q(2,L)^2+x^2-2xQ(2,L)\cos\psi(K,L)]$$
$$\left.\times K_2\left[\frac{3\pi}{8}\sqrt{Q(2,L)^2+x^2-2xQ(2,L)\cos\psi(K,L)}\right]dx\right) \ , \tag{57}$$

with $Q(K,L) = |\vec{Q}(K,L)|$.

From the eikonal function $\widetilde{\chi}$ we contruct the loop-loop amplitude $\widetilde{J}^{MM'}(\vec{b},\vec{R}_1,\vec{R}_2)$ following Eq. (36), where $\vec{R}_1$ and $\vec{R}_2$ are shorthand notation for $\vec{R}(1,1)$ and $\vec{R}(2,1)$, respectively. The meson-meson scattering amplitude is then constructed by averaging over the transverse wave functions, according to Eq. (41).

These results apply equally well to meson-baryon and baryon-baryon scattering if the baryon is represented as a mesonlike structure in the quark-diquark picture.

The evaluation of the eikonal function and of the observables for the nonconfining correlator follows the same lines. Since this part of the correlator is not going to be used in the phenomenological analysis, we only present in the Appendix B the comparison between some corresponding quantities for the two cases, in order to exhibit their large differences.

In order to treat the baryon as a genuine three-body configuration, we have to start from the expression given in Eq. (45). The projection of the loops for meson-baryon scattering is shown in Fig. 6. In this case the relation between the scattering amplitude J and the eikonal functions χ is more complicated than Eq. (36). Let us now define $\widetilde{\chi}$ by

$$A_K \equiv \widetilde{\chi}(\vec{b},\vec{R}(1,K),\vec{R}(2,1))$$
$$= -\cos\psi(K,1)\ I[Q(1,K),Q(2,1),\psi(K,1)]$$
$$+\cos\psi(K,2)\ I[Q(1,K),Q(2,2),\psi(K,2)] \ , \tag{58}$$

with the functions I given by Eq. (57). The index $K = 1,2,3$ refers to the three quarks in the baryon loop, which is here taken as hadron number 1. As before, in the meson loop (hadron number 2) the quark is labeled 1, the antiquark is labeled 2. The relevant quantity for the transition probability is then

$$\widetilde{J}_{BM}[\vec{b},\vec{R}(1,1),\vec{R}(1,2),\vec{R}(1,3),\vec{R}(2,1)] = \frac{-1}{144\times 8\times N_C^2(N_C^2-1)}(A_1^2+A_2^2+A_3^2-A_2A_3-A_1A_3-A_1A_2) \ . \tag{59}$$

For the scattering between two baryons in the three-body picture we define $\widetilde{\chi}$ by

$$\widetilde{\chi}(\vec{b},\vec{R}(1,K),\vec{R}(2,L)) \equiv A_{KL} = -\cos\psi(K,L)\ I[Q(1,K),Q(2,L),\psi(K,L)] \ , \tag{60}$$

which obviously represents the contribution due to the interaction between the quark loop K in baryon 1 and the quark loop L in baryon 2. Then the hadron-hadron scattering amplitude is given by

$$\tilde{J}_{BB}[\vec{b},\vec{R}(1,1),\vec{R}(1,2),\vec{R}(1,3),\vec{R}(2,1),\vec{R}(2,2),\vec{R}(2,3)]$$

$$= \frac{-1}{144\times 8\times N_C^2(N_C^2-1)}\Big[A_{11}^2+A_{12}^2+A_{13}^2+A_{21}^2+A_{22}^2+A_{23}^2+A_{31}^2+A_{32}^2+A_{33}^2$$
$$-A_{12}A_{13}-A_{22}A_{23}-A_{32}A_{33}-A_{11}A_{13}-A_{21}A_{23}-A_{31}A_{33}$$
$$-A_{11}A_{12}-A_{21}A_{22}-A_{31}A_{32}-A_{21}A_{31}-A_{22}A_{32}-A_{23}A_{33}$$
$$-A_{11}A_{31}-A_{12}A_{32}-A_{13}A_{33}-A_{11}A_{21}-A_{12}A_{22}-A_{13}A_{23}$$
$$+\frac{1}{2}\Big(A_{22}A_{33}+A_{23}A_{32}+A_{21}A_{33}+A_{23}A_{31}+A_{21}A_{32}+A_{22}A_{31}$$
$$+A_{12}A_{33}+A_{13}A_{32}+A_{11}A_{33}+A_{13}A_{31}+A_{11}A_{32}+A_{12}A_{31}$$
$$+A_{12}A_{23}+A_{13}A_{22}+A_{11}A_{23}+A_{13}A_{21}+A_{11}A_{22}+A_{12}A_{21}\Big)\Big] . \quad (61)$$

In the simplest case we place the quarks around the central point of the baryon in such a way that the vectors $\vec{R}(1,K)$ form angles of 120° (this configuration minimizes the string tension), and also choose the distances to the baryon center to be all equal, i.e., $|\vec{R}(1,1)| = |\vec{R}(1,2)| = |\vec{R}(1,3)|$. In this way, to form the amplitude, the configuration of the loops forming a baryon is specified by only one transverse vector, say $\vec{R}(1,1)$ of quark 1.

For the hadron transverse wave function we make the ansatz of the simple Gaussian form

$$\psi_H(R) = \sqrt{2/\pi}\frac{1}{S_H}\exp\left(-R^2/S_H^2\right) , \quad (62)$$

where S_H is a parameter for the hadron size.

Analogously to Eq. (41), we write the reduced hadron-hadron amplitude as an average over the hadronic wave functions

$$\hat{J}_{H_1H_2}(\vec{b},S_1,S_2) = \int d^2\vec{R}_1\int d^2\vec{R}_2\ \tilde{J}_{H_1H_2}(\vec{b},\vec{R}_1,\vec{R}_2)$$
$$\times|\psi_1(\vec{R}_1)|^2|\psi_2(\vec{R}_2)|^2 , \quad (63)$$

which is a dimensionless quantity.

The hadron-hadron scattering amplitude in the eikonal approach is then given by

$$T_{H_1H_2} = is[\kappa\langle g^2FF\rangle]^2a^{10}\int d^2\vec{b}\,\exp\left(i\vec{q}\cdot\vec{b}\right)$$
$$\times\hat{J}_{H_1H_2}(\vec{b},S_1,S_2) , \quad (64)$$

where the impact parameter vector $\vec{b}$ is in units of the correlation length a, and $\vec{q}$ is the momentum transfer projected on the transverse plane (in units of $1/a$, so that the momentum transfer squared is $t = -|\vec{q}|^2/a^2$). The eikonal approach requires large s and $|t| \ll s$.

We have verified that the contributions of next order in $\langle g^2FF\rangle$ are small [26], which is a consequence of the presence of the color factor in Eq. (36).

Our normalization for $T_{H_1H_2}$ is such that the total cross section is obtained through the optical theorem by

$$\sigma^T = \frac{1}{s}\,\mathrm{Im}\,T_{H_1H_2} , \quad (65)$$

and the differential cross section is given by

$$\frac{d\sigma^{el}}{dt} = \frac{1}{16\pi s^2}\,|T_{H_1H_2}|^2 . \quad (66)$$

For short, from now on we write $J(b)$ to represent $\hat{J}(\vec{b},S_1,S_2)$.

The shapes of $J(b)$ for the three cases of hadronic scattering are shown in Fig. 7, against the impact parameter

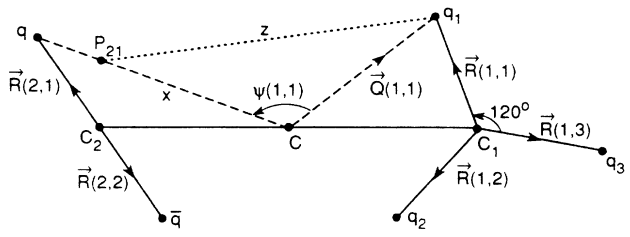

FIG. 6. Geometrical variables for the calculation of the eikonal function for meson-baryon scattering. Notation analogous to Fig. 5.

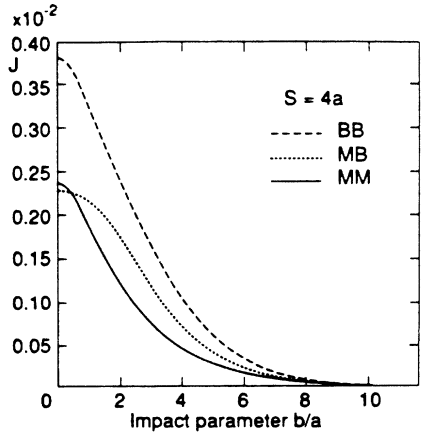

FIG. 7. Dimensionless function $\hat{J}(b/a)$, where b is the impact parameter, and a is the correlation length. The three represented cases refer to baryon-baryon (BB), meson-baryon (MB), and meson-meson (MM) amplitudes, with the same values ($S_1 = S_2 = S = 4a$) for the hadron extension parameters.

b (in units of the characteristic length a). In all the three curves represented in the figure, we have used $S/a = 4$ for both interacting hadrons. The label M means mesonlike structure, while B means a three-body configuration.

In all cases, $J(b/a)$ can be written, in very good approximation, as a function of the form

$$\hat{J}(b) = J(0)\,\frac{P_1 + P_2(b/a)^2}{P_1 + (b/a)^2}\,\exp\left[-P_3(b/a)^2\right], \qquad (67)$$

where P_1, P_2, P_3 are parameters, determined by fitting the exact (numerically obtained) values of $J(b/a)$.

Let us define the dimensionless quantities (as before, with b in units of the correlation length a)

$$I_k = \int d^2\vec{b}\; b^k\; \hat{J}(b), \quad k = 0, 1, 2, \ldots \qquad (68)$$

which depend only on S/a, and the Fourier-Bessel transform

$$I(t) = \int d^2\vec{b}\; J_0(ba\sqrt{|t|})\; \hat{J}(b)\;, \qquad (69)$$

where $J_0(ba\sqrt{|t|})$ is the zeroth-order Bessel function. Thus

$$T_{H_1H_2} = is[\kappa\langle g^2FF\rangle]^2 a^{10} I(t)\;.$$

Since $J(b)$ is real, the total cross section σ^T, the differential elastic cross section and the slope parameter (slope at $t = 0$)

$$B = \frac{d}{dt}\left(\ln\frac{d\sigma^{el}}{dt}\right)\Big|_{t=0}, \qquad (70)$$

are given by

$$\sigma^T = I_0[\kappa\langle g^2FF\rangle]^2 a^{10}\;, \qquad (71)$$

$$\frac{d\sigma}{dt} = \frac{1}{16\pi} I(t)^2\;[\kappa\langle g^2FF\rangle]^4 a^{20}\;, \qquad (72)$$

and

$$B = \frac{1}{2}\,\frac{I_2}{I_0}\,a^2 = Ka^2. \qquad (73)$$

We have here defined

$$K = \frac{1}{2}\,\frac{I_2}{I_0}\;, \qquad (74)$$

which is a function of S_1/a and S_2/a only.

We observe that in the lowest order of the correlator expansion used here, the slope parameter B does not depend on the value of the gluon condensate $\langle g^2FF\rangle$.

The curves for $I_0 = \sigma^T/\left[(\kappa g^2\langle FF\rangle)^2 a^{10}\right]$ and for $K = B/a^2$ as functions of S/a are shown respectively in Figs. 8 and 9, for the BB, MM, and MB cases, with hadrons of same extensions, $S_1 = S_2 = S$.

In the interesting ranges $1 \le S/a \le 3$ and $0.5 \le S_2/S_1 \le 1$, parametrizations for the dependence of the total cross section and slope parameter on the hadron size parameters S_i, to an accuracy better than 3% are

$$I_0 = \alpha\left(\frac{S_1S_2}{a^2}\right)^{\beta/2} \qquad (75)$$

and

$$B = 1.558a^2 + (\gamma/2)[S_1^2 + S_2^2]\;, \qquad (76)$$

where the value of the constants α, β, γ are given in Table I for the three different cases.

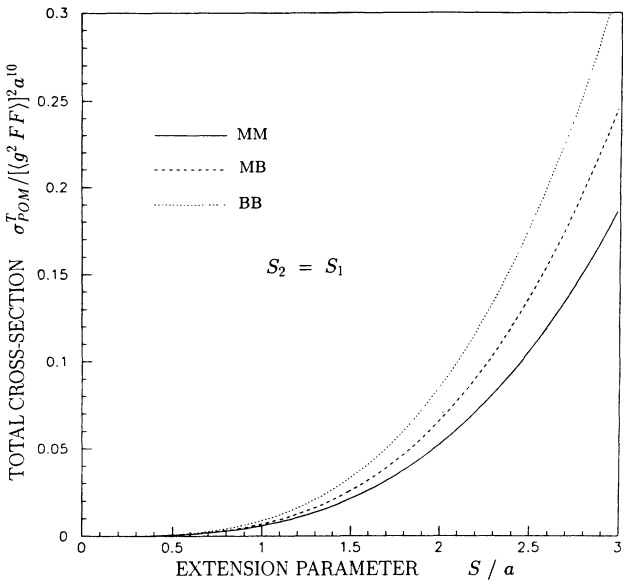

FIG. 8. Function $I_0(S/a)$ representing the dependence of the total cross section on the extension parameter S (in units of the correlation length a) of the hadron wave function. M represents a mesonlike hadronic configuration ($q\bar{q}$ for mesons, quark-diquark for baryons), and B represents a three-body starlike picture for baryons. We have here used $S_1 = S_2 = S$ in all cases.

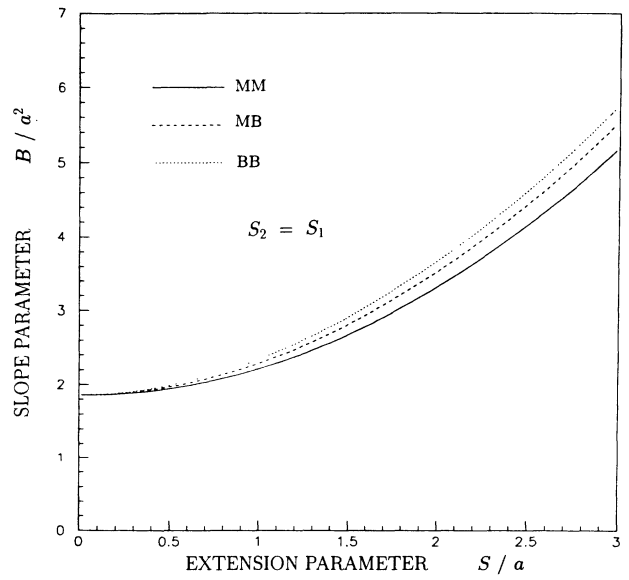

FIG. 9. Same as for previous figure, for the quantity $K(S/a)$, which represents the slope parameter B divided by a^2.

TABLE I. Values of the parameters to be used in Eqs. (75) and (76) to determine total cross sections and slopes.

Case	α	β	γ
MM	0.00626	3.090	0.366
BB	0.00881	3.277	0.454
BM	0.00682	3.135	0.348

A more precise parametrization, accurate in ranges of S_1/a extending from 0 to 5, is given by

$$I_0 = \alpha\left(\frac{S_1}{a}\right)^{\beta} \tag{77}$$

and

$$K = 1.558 + \gamma\left(\frac{S_1}{a}\right)^{\delta}, \tag{78}$$

where now the coefficients α and γ depend on the ratio S_2/S_1. The values of the parameters $\alpha, \beta, \gamma, \delta$ are given in Table II, for values of the ratios S_2/S_1 which we consider in the next section, where, besides pp and $\bar{p}p$ scattering, we also discuss $p\pi$, pK, and $p\Sigma$ scattering, in which cases $S_2 \neq S_1$.

The t dependence of the logarithmic slope of the differential cross section is given by

$$\begin{aligned} B(t) &= \frac{d}{dt}\left(\ln\frac{d\sigma^{el}}{dt}\right) \\ &= \frac{2}{I(t)}\frac{dI(t)}{dt} \\ &= \frac{a^2}{I(t)}\int_0^{\infty}\frac{2\pi}{\sqrt{|t|}}J(b)b^2J_1(ba\sqrt{|t|})db\ . \end{aligned} \tag{79}$$

For small t values, we obtain, expanding the Bessel function,

$$\begin{aligned} B(t) &\simeq B(0)\left[1+\frac{1}{8}\left(\frac{2I_2}{I_0}-\frac{I_4}{I_2}\right)a^2|t|\right] \\ &\equiv B(0)[1+Ca^2|t|]\ . \end{aligned} \tag{80}$$

The values for C that we have obtained in our calculations for systems with $S_2 = S_1 = S$ are almost independent of S/a. The values are $C \simeq -0.54$ for MM systems (here is included the case of diquark picture for baryons) and $C \simeq -0.42$ for BB systems (three-body picture for hadrons).

V. CHOICE OF PARAMETERS AND COMPARISON WITH EXPERIMENT

The numerical parametrizations of the total cross section and of the slope parameter B, Eqs. (75) and (76), are very convenient for comparison of our model with experiment. We first concentrate on elastic pp and $p\bar{p}$ scattering. In these channels data are available over a wide energy range. Since phenomenologically the Regge-pole parametrization works very well [6,7], the vacuum exchange contribution, to which our model refers, can be extracted as the Pomeron contribution in a Regge-pole analysis. Donnachie and Landshoff [7] found that the parametrization

$$\sigma^T_{\rm Pom}(pp,\bar{p}p) = 21.70\ {\rm mb}\ s^{0.0808} \tag{81}$$

(with s in GeV) works very well over the whole range of data from $\sqrt{s} = 5$ to 1800 GeV, so that we can use this expression for the Pomeron contribution. According to our convention we choose as energy $\sqrt{s} = 20$ GeV, but we wish to enphasize already here that the value of the QCD parameters, namely the gluon condensate $\langle g^2FF\rangle$ and the correlation length a entering expressions (11) and (28) for the fundamental correlator, are practically independent of the choice of the energy value. We return to this point at the end of this section.

For the value of the logarithmic slope of the elastic cross section at $t = 0$ for $\sqrt{s} = 20$ GeV we use [4]

$$B = 12.47 \pm 0.10\ {\rm GeV}^{-2}\ . \tag{82}$$

This value extrapolates very well, through a Regge amplitude with $\alpha'(0) = 0.25\ {\rm GeV}^{-2}$, to the observed [2] value $B = 17\ {\rm GeV}^{-2}$ at $\sqrt{s} = 1800$ GeV, so that it can be taken confidently as representative for the vacuum exchange contribution.

Once the form of the correlator is fixed, we have two parameters in the model, which are fundamentally related to QCD, namely the gluon condensate $\langle g^2FF\rangle$ and

TABLE II. Values of the parameters for Eqs. (77) and (78), for several values of S_2/S_1 which are important to represent the total cross sections and slopes for different hadronic systems.

Hadrons	1	2	Parameters for cross sections		Parameters for slopes	
			α	β	γ	δ
$S_2 = S_1$	M	M	0.006260	3.090	0.3616	2.023
	B	M	0.007846	3.135	0.4311	1.955
	B	B	0.008814	3.277	0.4891	1.892
$S_2 = 0.94S_1$	M	M	0.005610	3.090	0.3403	2.023
	B	B	0.008000	3.277	0.4636	1.892
$S_2 = 0.77S_1$	M	M	0.004159	3.090	0.2908	2.023
	B	M	0.004446	3.277	0.3577	1.955
$S_2 = 0.67S_1$	M	M	0.003353	3.090	0.2672	2.023
	B	M	0.003604	3.277	0.3330	1.955

the correlation length a, and the extension parameter S_H, determined by phenomenological hadronic physics. Of course none of these parameters is completely free, as they appear in other phenomena besides soft high-energy scattering, and they may be obtained also through lattice calculations. In this section we take advantage of this independent information to check the consistency and fix the values of our physical parameters.

The gluon condensate $\langle g^2FF\rangle$ was first determined in 1979 by Shifman, Vainshtein, and Zakharov [15] in the framework at QCD sum rules applied to the charmonium system, with a value $\langle g^2FF\rangle = 0.47$ GeV^4. The analysis has been repeated and extended many times, several authors finding a range of values extending to considerably larger values (see Appendix C). So we here accept as conservative estimate the range

$$\langle g^2FF\rangle = (0.5 - 1.5)\ \text{GeV}^4\ . \tag{83}$$

There are also theoretical uncertainties. Low-energy theorems [30] indicate that, in a world without light quarks, the condensate value would be larger by a factor 2 to 3 than the empirical value of our world with three light flavors. Therefore in our calculation we must refer to the value of the gluon condensate which is valid for a world without light quarks. Our model does not include dynamical effects of light quarks, which are treated as external sources moving on given (lightlike) paths. A consequence of the absence of dynamical fermions is that the fermion (or Wilson loop) renormalization constant is equal to 1. Taking into account dynamical fermions not only would change the value of the gluon condensate but also would lead to a loop renormalization constant [see Eq. (21)],

$$Z_\psi = \left\langle \frac{1}{N_c}\text{tr}\ W(0,\vec{\text{R}}) \right\rangle_A\ , \tag{84}$$

that is smaller than one. Thus in our case we should use a value for the gluon condensate from a pure gauge theory

$$\langle g^2FF\rangle = (1 - 3)\ \text{GeV}^4\ . \tag{85}$$

As already mentioned in Sec. II, the fundamental correlator

$$\langle F^C_{\mu\nu}(x,0)\ F^D_{\rho\sigma}(0,0)\rangle_A$$

has been calculated in a pure SU(3) lattice gauge theory by Di Giacomo and Panagopoulos [23] using the cooling method. By this method the high frequency contributions are frozen out and therefore this correlator is just the one which can be compared to that of our investigations. The cooling method works very well for Euclidean distances above about 0.4 fm and the results obtained in the lattice calculations show that the *confining* tensor structure $\{\delta_{\mu\rho}\delta_{\nu\sigma} - \delta_{\mu\sigma}\delta_{\nu\rho}\}$ in Eq. (11) is definitely present and even dominant, with $\kappa \sim 3/4$. In the physical range from $r = 0.5$ to $r = 0.8$ fm, the scalar function $\kappa\langle g^2FF\rangle D(-r^2/a^2)$ is given by the function

$$\kappa\langle g^2FF\rangle D(-r^2/a^2) = 24A\exp(-r/\lambda)\ , \tag{86}$$

with

$$A = 3.6\times 10^8\ \Lambda_L^4,\quad \lambda = 1/(183\Lambda_L)\ ,$$
and
$$\Lambda_L = (0.005 \pm 0.0015)\ \text{GeV}\ . \tag{87}$$

Within the given accuracy, the scalar function D_1 is proportional to D, and $\kappa \sim 3/4$. Our choice of the correlator function $D(z^2/a^2)$ given by Eq. (37) with $n = 4$, in the Euclidean region of the lattice results, namely for values $1 \le -z^2/a^2 \le 9$, is well approximated by an exponential function. We can therefore determine the gluon condensate and the correlation length a by fitting our expression for the correlator to the one obtained in the lattice calculation. The values obtained for $\kappa\langle g^2FF\rangle$ and a depend strongly on the value of the lattice-QCD parameter Λ_L. In Fig. 10 we show our correlator (solid line) together with the result found in the lattice calculation in the region $0.5 \le r \le 0.8$ fm, for the choice $\Lambda_L = 0.0044$ GeV. This fitting leads to the values $\kappa\langle g^2FF\rangle = 1.774$ GeV^4 and $a = 0.350$ fm.

With this value for a, our correlator passes through zero for $r \approx 1.4$ fm. This change of sign is certainly an artifact of our special ansatz, but is has no practical consequences, since it occurs in a region where the exponential damping makes its contribution irrelevant anyhow.

As mentioned in Sec. II B, the evaluation of the (Euclidean) Wilson loop in the model of the stochastic vacuum yields a relation involving the condensate $\kappa\langle g^2FF\rangle$, the correlation length a and the string tension ρ [see Eq. (15)]. For our family of correlators the integral can be performed analytically [see Eq. (40)] and we obtain for the case $n = 4$

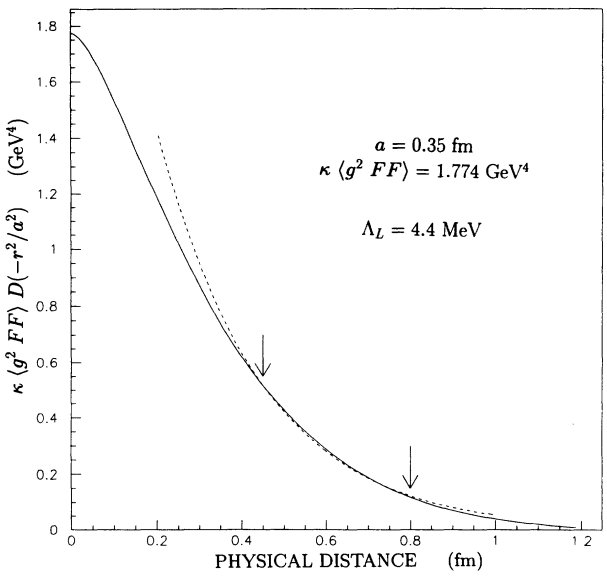

FIG. 10. Demonstration of the determination of the QCD parameters through the fitting of our correlator to the lattice calculation results [23], for a given value of Λ_L. Dashed line: lattice results for $\Lambda_L = 4.4$ MeV. The arrows indicate the range inside which the lattice calculations were made. Solid line: our fitted correlator, with the fitted values $a = 0.350$ fm and $\kappa\langle g^2FF\rangle D(-|\vec{\xi}|^2) = 1.772$ GeV^4 at $|\vec{\xi}| = 0$.

$$\kappa\langle g^2FF\rangle = \frac{81\pi}{8a^2}\rho \ . \tag{88}$$

Finally, we remark that the extension parameter S_p is not completely arbitrary, but should be in a range of values $S_p = 0.5, \ldots, 1$ fm, i.e., around the proton electromagnetic radius. We now use all this information to analyze our results.

In Fig. 11 we display the relation between the gluon condensate $\langle g^2FF\rangle$ and the correlation length a obtained from different sources. Figure 11(a) refers to the diquark picture and Fig. 11(b) to the three-body picture for the proton. The solid lines show the possible choices of $\langle g^2FF\rangle$ and a as obtained from our model, using Eqs. (71), (73), (75), and (76) and the experimental inputs $\sigma^T_{\rm Pom} = 34.9$ mb and $B = 12.47$ GeV^{-2}. To indicate the ranges of values of the proton radius which are represented in the plots, we mark on these curves the points where the values of S_p are 0.8 fm (three-body case), 0.9 fm (diquark case), and 0.6 fm (both cases).

The dashed lines represents the results of the lattice calculation [23], where the largest error comes from the uncertainty in the lattice QCD parameter $\Lambda_L = 5 \pm 1.5$ MeV. The values corresponding to some chosen values of Λ_L are marked on this curve. The points for this curve have been obtained by fitting the lattice results to our form for the correlator, as exemplified for a given value of Λ_L in Fig. 10.

The dotted lines represent the relation between the gluon condensate, the correlation length and the string tension as obtained in the model of the stochastic vacuum [10,11]; for our form of correlator, this relation is given by Eq. (88). The upper and lower dotted curves correspond, respectively, to string tension values $\rho = 0.18$ GeV^2 and 0.16 GeV^2.

As can be seen from the figures, the constraints from these three independent sources of information are simultaneously satisfied in a narrow region, providing a very consistent picture of soft high-energy pp and $\bar{p}p$ scattering, for the following sets of parameters.

(1) In the diquark picture

$$a = 0.350 \text{ fm} \ , \quad \langle g^2FF\rangle = 2.39 \text{ GeV}^4 \ , \quad S_p = 0.835 \text{ fm} \ ,$$
$$\Lambda_L = 4.4 \text{ MeV} \ , \quad \rho = 0.18 \text{ GeV}^2 \ . \tag{89}$$

(2) In the three-body picture

$$a = 0.361 \text{ fm} \ , \quad \langle g^2FF\rangle = 2.08 \text{ GeV}^4 \ , \quad S_p = 0.730 \text{ fm} \ ,$$
$$\Lambda_L = 4.2 \text{ MeV} \ , \quad \rho = 0.16 \text{ GeV}^2 \ . \tag{90}$$

The calculations described above lead to a determination of $\kappa\langle g^2FF\rangle$. To obtain the value of the full condensate quoted above, we have used $\kappa = 0.74$, as determined by the lattice calculation [23].

The (pure gauge) gluon condensate is well compatible with the canonical value [see (85)]. The resulting proton size parameter S_p comes out quite close to the electromagnetic radius [31] value, which is $R_p = 0.862 \pm 0.012$ fm. The lattice parameter Λ_L and the string tension ρ are also in their acceptable ranges.

A very specific feature of the model of the stochastic vacuum is the dependence of the total cross section on the hadron size, even if the latter is large as compared to the correlation length. The size dependence can best be tested by comparing the cross sections for different hadronic systems. The Donnachie-Landshoff parametrization [7] gives for the Pomeron parts of $p\pi$ and pK cross sections the ratios

$$\sigma_{p\pi}/\sigma_{pp} = 0.63, \quad \sigma_{pK}/\sigma_{p\pi} = 0.87 \ . \tag{91}$$

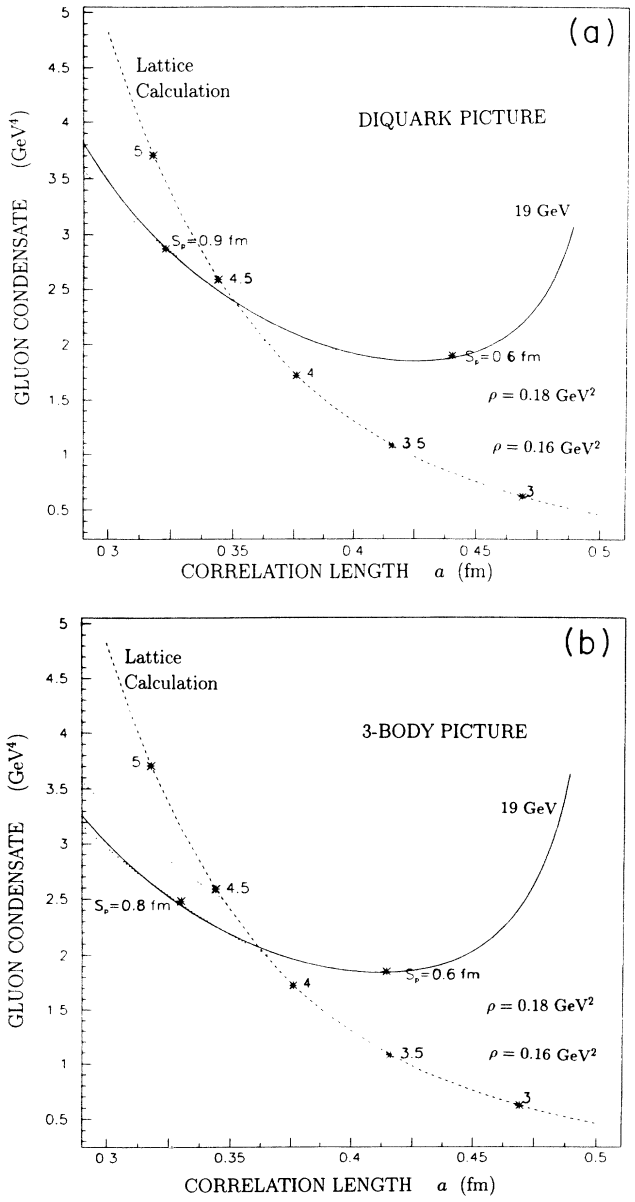

FIG. 11. (a) Constraints on the values of $\kappa\langle g^2FF\rangle$ and of the correlation length a. Solid line: our model of high energy scattering, with $\sigma^T_{pp} = 35$ mb and $B = 12.47$ GeV^{-2}, using a diquark picture for the proton; dashed line: fit of our correlator to the lattice calculation [23]; dotted lines: relation obtained from string tension ρ, Eq. (88), the upper curve corresponding to $\rho = 0.18$ GeV^2, and the lower one to $\rho = 0.16$ GeV^2. (b) Same as (a), for the case of a three-body picture for the proton.

In our treatment the theoretically predicted cross-section ratios depend on the hadron sizes. We take for the ratios of these sizes the ratios of the respective electromagnetic radii. The known values [31] for these radii are

$$R_p = 0.862 \pm 0.012 \text{ fm} , \quad R_\pi = 0.66 \pm 0.01 \text{ fm} , \quad R_K = 0.58 \pm 0.04 \text{ fm}. \tag{92}$$

With this input we obtain for the predicted ratios the results of Table III .

We see that in the diquark picture both ratios agree very well with experiment. In the three-body picture the $\sigma_{p\pi}/\sigma_{pp}$ ratio comes out too small. Presumably the assumption that the ratio of hadron radii is the same as the ratio of the electromagnetic radii is an oversimplification if the assumed structures for the mesons and baryons are so different, as when we relate $\sigma_{p\pi}$ with σ_{pp} with protons in the three-body picture. This is confirmed by the fact that both pictures reproduce perfectly well the $\sigma_{p\pi}/\sigma_{pK}$ ratio, where the effect of the three-body baryon structure is the same in both terms of the ratio, cancelling out.

With the criterium for the ratios of hadronic radii now fixed, we can also calculate the $\pi\pi$ cross section and we find that for both the diquark and the three-body picture the factorization relation

$$\sigma_{\pi\pi} = (\sigma_{p\pi})^2/\sigma_{pp} \tag{93}$$

is numerically perfectly fulfilled, as can be verified through the parameter values given in Table II. From the data on the pp and $p\pi$ systems we thus predict the Pomeron part of the $\pi\pi$ scattering cross section to be

$$\sigma_{\pi\pi} = 8.6 \text{ mb } s^{0.0808} . \tag{94}$$

The only experimental result, known to us, on the $\pi\pi$ cross section [32] gives $\sigma_{\pi\pi} = 10$ mb at $\sqrt{s} = 4$ GeV, while the above expression predicts 9.6 mb for the Pomeron part at this energy.

There are some data available on hyperon-proton scattering [5], which also fit nicely in the general picture. If we dare to extract a vacuum exchange part from the few existing data for Σp scattering, we obtain

$$\sigma_{p\Sigma^-} = 19.6 \text{ mb } s^{0.0808} . \tag{95}$$

From this cross section we obtain for the ratio of the extension parameters, in both the diquark and three-body pictures, the value

$$S_{\Sigma^-}/S_p = 0.94 , \tag{96}$$

which certainly is a reasonable result.

TABLE III. Ratios of the Pomeron exchange contributions to the total cross sections for different processes.

Cross-section ratios	p picture diquark	p picture three-body	Experimental values
$\sigma_{p\pi}/\sigma_{pp}$	0.66 ± 0.02	0.50 ± 0.02	0.63
$\sigma_{pK}/\sigma_{p\pi}$	0.82 ± 0.08	0.82 ± 0.08	0.87

The size dependence of the slope parameter at $t = 0$ is given in parametrized form by Eq. (76). In Table IV we show the results of our model for the differences of the slope parameters for pp, Σp, $p\pi$, and pK scattering. The extension parameters S_H for the different hadrons are assumed to be proportional to the electromagnetic radii given in Eq. (92). The experimental numbers for the vacuum exchange part of the slopes were taken from the analysis by Burq [4] (see their Table 7, extrapolated to $t = 0$ according to Table 8). The extrapolation to $t = 0$ has little effect on the value of the slope, for our purposes at this point.

Comparison with the data shows that the difference of the slopes for πp and pp scattering is underestimated in our model, while the difference for πp and Kp is well compatible with experiment.

The parametrization (76) of the slope parameter

$$B = 1.858\ a^2 + 0.183\ (S_1^2 + S_2^2) , \tag{97}$$

where S_1 and S_2 represent the hadron sizes, and a is the correlation length, is a good approximation, within a few percent, to the results of our model. This parametrization can be compared to that of a modified Chou-Yang picture [33], which allows also for a quark form factor

$$B = \frac{1}{3}(R_q^2 + R_1^2 + R_2^2) , \tag{98}$$

where R_q and R_i are the electromagnetic radii of the quark and hadrons, respectively. Since in our results $1.858a^2$ is about 6 GeV^{-2}, we see that in our model the correlation length a gives a much more important contribution to the slope than the quark form factor of the modified Chou-Yang model. These different predictions should be tested experimentally.

It is a curious result of our treatment that, given the ratios of the electromagnetic radii of the hadrons, the ratios of the differences of slope parameters are practically those of simple integers. Thus in the diquark picture

$$B_{p\pi} - B_{pK} : B_{pp} - B_{p\pi} : B_{pp} - B_{pK} : B_{pp} - B_{p\Sigma} = 1 : 3 : 4 : \frac{9}{10} . \tag{99}$$

We remark that the last figure in this sequence of ratios is a bit more uncertain than the three first ones, because it was determined using the poor Σp scattering data, and the predicted, not experimentally measured, ratio $(S_\Sigma/S_p) = 0.94$.

Our model also predicts a t dependence for the logarithmic slope parameter, as shown in Eq. (80). In the

TABLE IV. Differences of the logarithmic slopes of the Pomeron part at $t = 0$ for different processes, in GeV^{-2}.

Slopes	Diquark picture	Three-body picture	Experimental values
$B_{pp} - B_{\Sigma p}$	0.40	0.45	–
$B_{pp} - B_{\pi p}$	1.30	1.45	2.48
$B_{\pi p} - B_{Kp}$	0.43	0.34	0.34

analysis by Burq [4], the t depencence of the elastic cross sections has been written in the form

$$\frac{d\sigma}{dt} = \left.\frac{d\sigma}{dt}\right|_{t=0} e^{[B(0)+ct+dt^2]t} , \tag{100}$$

with the parametrization for $B(t)$

$$B(t) = B(0) - 2c|t| + 3d|t|^2 . \tag{101}$$

From Eq. (80) and our results for the slope of the slope C, we obtain for this parameter c the values

$$c = 10.6 \text{ GeV}^{-4} \quad \text{in the diquark picture} , \tag{102}$$

$$c = 8.8 \text{ GeV}^{-4} \quad \text{in the three-body picture} . \tag{103}$$

These values are to be compared with the experimental value 6.8 ± 0.5 GeV^{-4} obtained by Burq [4]. However we should not overestimate the significance of this comparison. On the theoretical side this slope of the slope depends strongly on the precise form of the profile function $J(b)$, while the experimental results are not accurate and may still be contaminated by Coulomb interference.

If we consider hadron-hadron scattering for two hadrons of equal sizes, we can eliminate the hadron radius between the parametrized forms for σ^T and B, and obtain the relation

$$\sigma^T_{\text{Pom}} = \alpha\gamma^{-\beta/\delta}(\kappa\langle g^2FF\rangle)^2 a^{10-2\beta/\delta}(B - 1.858a^2)^{\beta/\delta} , \tag{104}$$

where the values for the model dependent parameters $\alpha, \beta, \gamma, \delta$ are given in Table II.

If we fix $\kappa\langle g^2\ FF\rangle$ and a at one given energy (e.g., $\sqrt{s} = 20$ GeV), we obtain through Eq. (104) a parameter-free relation between the total cross section σ^T_{Pom} and the slope parameter B.

In Fig. 12 we display σ^T_{Pom} against B as given by Eq. (104), for both diquark and three-body pictures for the proton, using the sets of parameters given in Table II. In the same figure we also show the relation

$$\sigma^T_{\text{Regge}} = \sigma^T_0\ e^{0.1616(B-B_0)} , \tag{105}$$

obtained from a Regge amplitude using the slope of the Pomeron trajectory $\alpha'(0)_{\text{Pom}} = 0.25$ GeV^{-2}, and as input at $\sqrt{s} = 20$ GeV the values $\sigma^T_0 = 35$ mb, and $B_0 = 12.47$ GeV^2 . The experimental data [2] at 540 GeV and 1800 GeV are marked in the plot, together with the input data at 20 GeV. We observe that our relation (104), which contains no free parameters, describes the experimentally observed relation between B and σ^T astonishingly well. Besides, there is a surprising agreement between the Regge parametrization line and our results. It must be remarked that the constant term $1.858a^2$ in our expression for the slope B is important for this good agreement with experiment.

The application of our results to different energies implies a very slow energy dependence of the hadronic radii. An explicit relation is obtained if we bring into Eqs. (71) and (77) a parametrization for the energy dependence of the total cross sections, such as the Donnachie-Landshoff

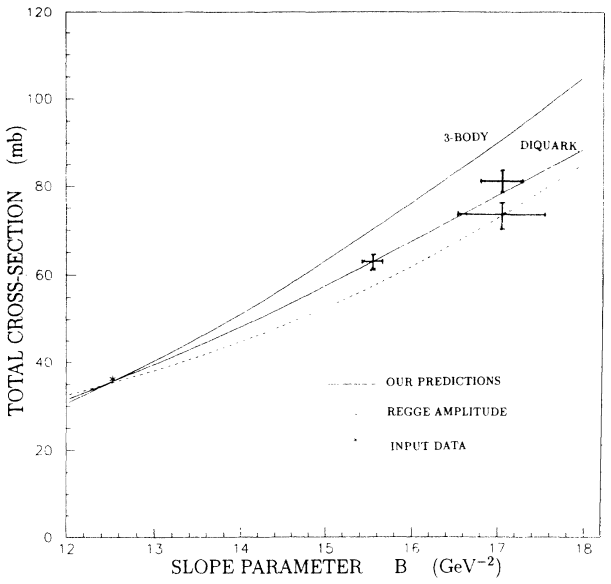

FIG. 12. Relation between the total cross section and the slope parameter B. Solid lines: predictions given by Eq. (104), obtained from our model by eliminating the hadronic size, in the cases of diquark and three-body pictures for the proton; dashed line: relation obtained from the Regge amplitude with $\alpha(0) = 1.0808$ and $\alpha'(0) = 0.25$ GeV^{-2}; star: input data at $\sqrt{s} = 19$ GeV; crosses: experimental data at 541 and 1800 GeV.

[7] form of Eq. (81). We thus obtain for the proton radius

$$S_p(s) = a\left[\frac{\kappa\langle g^2FF\rangle^2 a^{10}(21.7 \text{ mb})}{0.00626}\right]^{1/3.090} s^{0.0808/3.090} \tag{106}$$

in the diquark picture, and

$$S_p(s) = a\left[\frac{\kappa\langle g^2FF\rangle^2 a^{10}(21.7 \text{ mb})}{0.00881}\right]^{1/3.277} s^{0.0808/3.277} \tag{107}$$

in the three-body configuration case. The values thus obtained for S_p are in the region of the proton electromagnetic radius.

VI. CONCLUSIONS

We have obtained a very consistent description of the data on soft high-energy scattering. Our basic assumption is that the low frequency, i.e., nonperturbative, contributions to the scattering amplitudes can be approximated by a Gaussian process. The parameters determining the observable quantities are the gluon condensate and the correlation length of the vacuum field fluctuations. These parameters occur also in completely different connections (SVZ sum rules, lattice calculations, low-energy hadron spectroscopy), and all the conditions posed on them can be consistently satisfied. The

third parameter entering our calculations is the transverse hadron size, which may be related to the electromagnetic radius.

Gauge invariance is observed on each step of the calculation, which is based on a formalism for loop-loop scattering, rather than on a quark-quark scattering picture. In this way even finite distance correlations of the vacuum field tensor lead to long range correlations that are the common source of confinement, and to a dependence of the total scattering cross section on the hadron size. This mechanism can be interpreted as a string-string interaction in hadronic scattering.

The size dependence of the cross sections leads to a natural explanation for the experimentally observed flavor dependence of the total cross section. The ratio between the pion-proton and (anti)proton-proton cross sections emerges in our model as a consequence of the different hadron sizes, and the factor $2/3$ comes out as a consequence of the ratio of the electromagnetic radii, and not from quark additivity.

The size dependence of the slope parameter, i.e., the logarithmic slope of the differential elastic cross section, can be parametrized in a form similar to that of a modified Chou-Yang model [33] with a finite quark radius, which in our model appears as a correlation length.

Elimination of the extension parameter yields a parameter-free relation between the total cross section and the slope of the elastic cross section which agrees very well with experiment.

The investigations described in this paper can be extended in many directions. In the present calculations only one of the two possible tensor structures determining the low frequency contributions is taken into account. The inclusion of the second term, which could also describe perturbative effects (and even Coulomb interaction), would pose no important technical problems. Furthermore, we have restricted ourselves to the lowest-order nonvanishing contribution, which is quadratic in the gluonic correlator. We have checked that this is justified for the total cross section and the slope parameter. But our amplitude is purely imaginary, and quantities like the ρ parameter (the ratio of the real to the imaginary parts of the elastic scattering amplitude) can only be described if we go one further order in the contributions to the correlator.

A further important step to be developed is the test of the importance of the factorization implied by the assumption of a Gaussian process. This is certainly crucial in the present investigation, with possible consequences for the phenomenological analysis, but it remains to be seen which of the more general features depend on this approximation.

It would of course be highly desirable improve the present model in order to describe the dependence of the cross section with the energy. However, although we cannot obtain the (slow) rise of the total cross section with the energy, we can eliminate the hadron radius parameter S and obtain a parameter-free relation between the total cross section and the slope parameter B, as shown in Fig. 12.

ACKNOWLEDGMENTS

We thank Adriano Di Giacomo, Peter Landshoff, Otto Nachtmann, and Yuri Simonov for many fruitful discussions and constructive critical remarks. We are also indebted to Otto Nachtmann for a critical reading of the manuscript. Part of this work has been done when two of the authors were visiting CERN. They (H.G.D. and E.F.) wish to thank the Theory Division for the hospitality. The same authors also thank CNPq (Brasil) and DAAD (Federal Republic of Germany) for the financial support. One of the authors (A.K.) gratefully acknowledges the support received from Studienstiftung des Deutschen Volkes.

APPENDIX A: THE CORRELATION FUNCTIONS

In Eqs. (11) and (28) there appear two independent arbitrary scalar functions, $D(z^2/a^2)$ and $D_1(z^2/a^2)$, which are supposed to fall off at large distances with characteristic lengths a, called correlation lengths, and must have forms that can be analytically continued from Euclidean to Minkowski space-time descriptions of field theory. If the expression for the correlator is used in Euclidean QCD, the scalar function $D(z^2/a^2)$, which is zero in Abelian theories (if there are no monopoles) leads to a linearly rising potential, namely to confinement. QCD lattice calculations have shown that the dominant contribution to the correlator actually comes from the term with $D(z^2/a^2)$, namely $\kappa \simeq 1$. Besides that, in Appendix B we show that the nonconfining part D_1 of the correlator has much less influence on the values of the eikonal functions of high-energy scattering. Consequently, in the present work we take into account only the confining term $D(z^2/a^2)$, with the weight κ determined by the lattice calculations, neglecting the effect of $D_1(z^2/a^2)$ altogether.

We thus concentrate on $D(z^2/a^2)$, and take as an ansatz the family of functions

$$D^{(n)}(\xi^2) = -6i \int \frac{d^4k}{(2\pi)^4} \frac{A_n k^2}{(k^2-1)^n} \exp(-ik\xi/\lambda_n) , \quad n \geq 4 , \quad \text{(A1)}$$

where

$$\xi = z/a , \quad \text{(A2)}$$

a is the characteristic correlation length, and the constants A_n and λ_n are to be fixed by normalization. It is convenient to absorb λ_n into k through $k/\lambda_n \to k$; then ξ,k and λ_n are all dimensionless. In the Euclidean metric

$$-id^4k = d^4K, \quad K_4 = ik_0, \quad k^2 = -K^2 = -(|\vec{\mathrm{K}}|^2 + K_4^2) , \quad \text{(A3)}$$

for spacelike vectors

$$\xi(0,\vec{\xi}=\sqrt{-\xi^2}\vec{e}_3)\ ,\quad \xi^2=-|\vec{\xi}|^2\ , \tag{A4}$$

we have

$$D^{(n)}(\xi^2)=D^{(n)}(-|\vec{\xi}|^2) =6(-1)^{n+1}\int\frac{d^4K}{(2\pi)^4}\ \frac{A_n\lambda_n^6K^2}{(\lambda_n^2K^2+1)^n} \times\exp(i\vec{K}\cdot\vec{\xi})\ . \tag{A5}$$

The constants A_n and λ_n can be fixed by the normalization conditions

$$D^{(n)}(0)=1,\quad \int_0^\infty d(|\vec{\xi}|)\ D^{(n)}(-|\vec{\xi}|^2)=1\ . \tag{A6}$$

The second of these two relations has the role of a definition for the correlation length.

These calculations can be made analytically, leading to

$$A_n=(-1)^{n+1}\frac{4\pi^2}{3}(n-1)(n-2)(n-3)\ , \tag{A7}$$

and

$$\lambda_n=\frac{1}{\rho_n}=\frac{4}{3\sqrt{\pi}}\frac{\Gamma(n-3)}{\Gamma(n-5/2)}\ . \tag{A8}$$

For simplicity of notation, from now on we use more often $\rho_n=1/\lambda_n$, instead of λ_n.

The integrations in Eq. (A5) can be performed analytically. We obtain

$$D^{(n)}(-|\vec{\xi}|^2)=\frac{(-1)^{n+1}3A_n}{\pi^2 2^{n-1}\Gamma(n)}(\rho_n|\vec{\xi}|)^{n-3} \times\left[(n-1)K_{n-3}(\rho_n|\vec{\xi}|) -\frac{1}{2}(\rho_n|\vec{\xi}|)K_{n-2}(\rho_n|\vec{\xi}|)\right]\ , \tag{A9}$$

which is the general form for the class of functions considered. $K_\nu(x)$ is the modified Bessel function.

Alternative useful forms to Eq. (A9) are

$$D^{(n)}(-|\vec{\xi}|^2)=\frac{(-1)^{n+1}3A_n}{\pi^2 2^n\Gamma(n)}\left(\rho_n|\vec{\xi}|\right)^{-3}\frac{d}{d(\rho_n|\vec{\xi}|)} \times\left[(\rho_n|\vec{\xi}|)^{n+1}K_{n-3}(\rho_n|\vec{\xi}|)\right]\ , \tag{A10}$$

and

$$D^{(n)}(-|\vec{\xi}|^2)=\frac{(-1)^n3A_n}{\pi^2 2^n\Gamma(n)}(\rho_n|\vec{\xi}|)^{-3}\frac{d}{d(\rho_n|\vec{\xi}|)} \times\left[(\rho_n|\vec{\xi}|)^3\frac{d}{d(\rho_n|\vec{\xi}|)}[(\rho_n|\vec{\xi}|)^{n-2} \times K_{n-2}(\rho_n|\vec{\xi}|)]\right]\ . \tag{A11}$$

These correlation functions are negative at large distances, behaving like

$$D^{(n)}(-|\vec{\xi}|^2)\simeq-\frac{\sqrt{\pi/2}}{2^{n-2}\Gamma(n-3)}(\rho_n|\vec{\xi}|)^{n-5/2}\exp(-\rho_n|\vec{\xi}|)\ . \tag{A12}$$

After the limits are taken, which make the long sides of the rectangular Wilson loops tend to $\pm\infty$ in the x_3 direction, the remaining variables in the integrands are coordinates of points in the transverse plane. The distances z between such points enter in the final expressions for the eikonal functions χ as arguments of the two-dimensional inverse Fourier transform of $\tilde{D}(k^2)$ in Eq. (37), which is defined by

$$\mathcal{F}_2^{(n)}(-|\vec{\xi}|^2)=-\frac{1}{(2\pi)^2}\int d^2\vec{K}_\perp\ \frac{6A_n\lambda_n^6|\vec{K}_\perp|^2}{(-\lambda_n^2|\vec{K}_\perp|^2-1)^n} \times\exp(i\vec{K}_\perp\cdot\vec{\xi})\ , \tag{A13}$$

where $\vec{\xi}$ is any two-dimensional vector of the transverse plane.

Using the values for A_n and ρ_n written above, we obtain

$$\mathcal{F}_2^{(n)}(-|\vec{\xi}|^2)=\frac{2^{(8-n)}\Gamma(n-3)}{9[\Gamma(n-5/2)]^2}(\rho_n|\vec{\xi}|)^{n-2} \times\left[(n-1)K_{n-2}(\rho_n|\vec{\xi}|) -\frac{1}{2}(\rho_n|\vec{\xi}|)K_{n-1}(\rho_n|\vec{\xi}|)\right]\ . \tag{A14}$$

Important alternative forms are

$$\mathcal{F}_2^{(n)}(-|\vec{\xi}|^2)=\frac{2^{(7-n)}\Gamma(n-3)}{9[\Gamma(n-5/2)]^2}(\rho_n|\vec{\xi}|)^{-1}\frac{d}{d(\rho_n|\vec{\xi}|)} \times\left[(\rho_n|\vec{\xi}|)^nK_{n-2}(\rho_n|\vec{\xi}|)\right]\ , \tag{A15}$$

and

$$\mathcal{F}_2^{(n)}(-|\vec{\xi}|^2)=-\frac{2^{(7-n)}\Gamma(n-3)}{9[\Gamma(n-5/2)]^2}(\rho_n|\vec{\xi}|)^{-1}\frac{d}{d(\rho_n|\vec{\xi}|)} \times\left[(\rho_n|\vec{\xi}|)\frac{d}{d(\rho_n|\vec{\xi}|)} \times\left((\rho_n|\vec{\xi}|)^{n-1}K_{n-1}(\rho_n|\vec{\xi}|)\right)\right]\ , \tag{A16}$$

or

$$\mathcal{F}_2^{(n)}(-|\vec{\xi}|^2)=-\frac{2^{(7-n)}\Gamma(n-3)}{9(\Gamma(n-5/2))^2}\Delta_2\psi^{(n)}(\rho_n|\vec{\xi}|)\ , \tag{A17}$$

where

$$\psi^{(n)}(\rho_n|\vec{\xi}|)\equiv(\rho_n|\vec{\xi}|)^{n-1}K_{n-1}(\rho_n|\vec{\xi}|)\ , \tag{A18}$$

and Δ_2 is the two-dimensional Laplacian operator. This Laplacian form is important in our calculation, as it allows lowering the order of the integrations, through Gauss theorem.

The moments of the $D^{(n)}(-|\vec{\xi}|^2)$ and $\mathcal{F}_2^{(n)}(-|\vec{\xi}|^2)$ functions can be readily obtained from Eqs. (A10) and (A15), respectively. For $D^{(n)}$ we obtain

$$\mathcal{M}_p[D^n(-|\vec{\xi}|^2)] = \int_0^\infty (\rho_n|\vec{\xi}|)^p \; D^{(n)}(-|\vec{\xi}|^2) d(\rho_n|\vec{\xi}|)$$
$$= 2^{p-2}(3-p)\frac{\rho_n^{-p+1}}{\Gamma(n-3)}\Gamma\left(\frac{p+1}{2}\right) \times\Gamma\left(n+\frac{p-5}{2}\right), \quad \text{(A19)}$$

where we observe that $\mathcal{M}_3[D^n(-|\vec{\xi}|^2)] = 0$ and that all moments higher than $p = 3$ are negative, for every n. Thus all correlation functions have a zero.

For $\mathcal{F}_2^{(n)}$ we have the moments

$$\mathcal{M}_p[\mathcal{F}_2^{(n)}(-|\vec{\xi}|^2)] = \int_0^\infty (\rho_n|\vec{\xi}|)^p \; \mathcal{F}_2^{(n)}(-|\vec{\xi}|^2) d(\rho_n|\vec{\xi}|)$$
$$= \frac{2^{(p+4)}}{9}(1-p)\frac{\rho_n^{-p+1}\Gamma(n-3)}{[\Gamma(n)]^2} \times\Gamma\left(\frac{p+1}{2}\right)\Gamma\left(n+\frac{p-3}{2}\right) . \quad \text{(A20)}$$

Thus for every n the moment $p = 1$ vanishes, and all higher moments are negative. Thus all $\mathcal{F}_2^{(n)}$ functions pass through zero.

We must choose the value of n in order to fix a specific form of the ansatz for the correlation function. Actually, the dependence of the final results on this particular choice has been tested [26], and found to be not very marked. The reason is that all correlation functions are normalized to 1 at the origin, and decrease exponentially at large distances. It is enough that the chosen function falls monotonically and smoothly in the range of physical influence (up to about 1 fm, say), and there cannot be much difference in the results obtained using different analytical forms. Of course there will be differences in the specific values given to the correlation length parameter a, due to the different values of the multiplicative factor ρ_n in the argument of the exponential behaviour [see Eq. (A12)], but such differences can be taken into account and absorbed when different forms of correlation functions are compared.

In the present work we make the choice that n=4, which in the Euclidean region leads to a good representation of the lattice calculations [23]. We then have for the correlation function

$$D^{(4)}(-|\vec{\xi}|^2) = (\rho_4|\vec{\xi}|)\left[K_1(\rho_4|\vec{\xi}|) - \frac{1}{4}(\rho_4|\vec{\xi}|)K_0(\rho_4|\vec{\xi}|)\right] \quad \text{(A21)}$$

and for the two-dimensional inverse Fourier transform

$$\mathcal{F}_2^{(4)}(-|\vec{\xi}|^2) = \frac{32}{9\pi}(\rho_4|\vec{\xi}|)^2\left[2K_0(\rho_4|\vec{\xi}|) - \left(\frac{4}{\rho_4|\vec{\xi}|} - \rho_4|\vec{\xi}|\right)K_1(\rho_4|\vec{\xi}|)\right]$$
$$= -\frac{32}{9\pi}\Delta_2[(\rho_4|\vec{\xi}|)^3 K_3(\rho_4|\vec{\xi}|)] , \quad \text{(A22)}$$

where

$$\rho_4 = \frac{3\pi}{8} . \quad \text{(A23)}$$

The functions $D^{(4)}(-|\vec{\xi}|^2)$, $\mathcal{F}_2^{(4)}(-|\vec{\xi}|^2)$, and $\psi^{(4)}(\rho_4|\vec{\xi}|)$ are represented in Figs. 13–15, against the variable $x = \rho_4|\vec{\xi}|$. The correlation function $D^{(4)}(-|\vec{\xi}|^2)$ has a zero at $\rho_4|\vec{\xi}| = 4.43$ while $\mathcal{F}_2^{(4)}(-|\vec{\xi}|^2)$ has a zero at $\rho_4|\vec{\xi}| = 3.05$. As we will see from our final results, the locations of these zeros are beyond the range of physical influence.

Practical representations for these functions, that are important for the numerical work, can be obtained. As a tool to obtain the parameters in approximate representations, we may use the moments of the functions, which are explicitly given by Eqs. (A19) and (A20). The function

$$\psi^{(4)}(x) = x^3 K_3(x) , \quad \text{(A24)}$$

where $x = \rho_4|\vec{\xi}|$, enters in heavy numerical computations to produce the eikonal functions. It appears in Eq. (57) as

$$\frac{d\psi}{dx} = -x^3 K_2(x) .$$

Let us write

$$\psi^{(4)}(x) \simeq 8\,[1 + x + a_1x^2 + a_2x^3 + a_3x_4]\; e^{-x} , \quad \text{(A25)}$$

that satisfies the constraints at the origin $\psi(0) = 8$ and $\psi'(0) = 0$. We then have

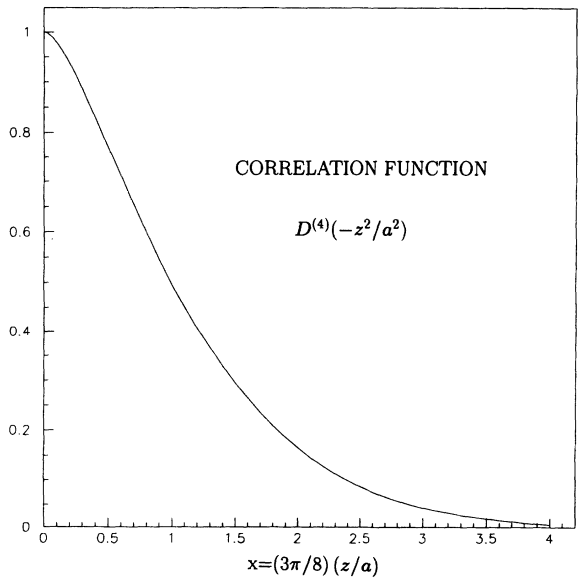

FIG. 13. Correlation function $D^{(4)}(-|\vec{\xi}|^2)$, given by Eq. (A21), against the variable $x = \rho_4|\vec{\xi}| = (3\pi/8)(z/a)$, where z is the physical distance, and a is the correlation length. The correlation function is normalized to one at the origin.

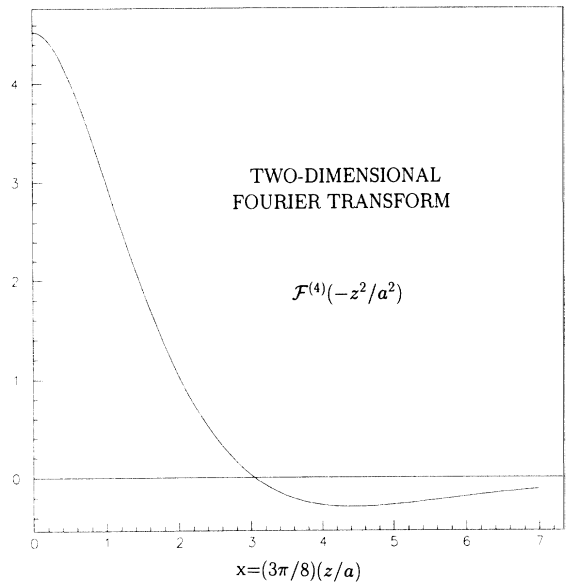

FIG. 14. Two-dimensional Fourier transform $\mathcal{F}_2^{(4)}(-|\vec{\xi}|^2)$, given by Eq. (A22), against $x = \rho_4|\vec{\xi}| = (3\pi/8)(z/a)$.

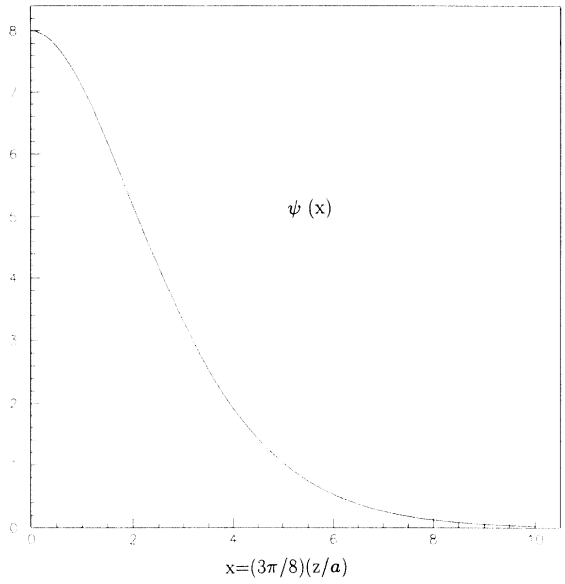

FIG. 15. Function $\psi^{(4)}(x) = x^3 K_3(x)$, given by Eq. (A23), and represented approximately through Eq. (A25).

$$\mathcal{F}_2^{(4)}(-|\vec{\xi}|^2) \simeq -\frac{2^8}{9\pi}\left[(-2+4a_1)+(1-5a_1+9a_2)x+(a_1-7a_2+16a_3)x^2+(a_2-9a_3)x^3+a_3x^4\right]e^{-x} . \quad \text{(A26)}$$

Using properties of $\mathcal{F}_2^{(4)}(-|\vec{\xi}|^2)$, we obtain

$$\begin{aligned}
&\mathcal{F}_2^{(4)}(x=0) = 2^7/(9\pi) \implies a_1 = 3/8 ,\\
&\left[\frac{d}{dx}\mathcal{F}_2^{(4)}\right](x=0) = 0 \implies a_2 = 1/24 ,\\
&\int_0^\infty \mathcal{F}_2^{(4)}dx = 16/3 \implies a_3 = \frac{1}{8}\left(\frac{7}{3}-\frac{3\pi}{4}\right) ,\\
&\int_0^\infty x\,\mathcal{F}_2^{(4)}dx = 0 \implies \text{identity} . \qquad \text{(A27)}
\end{aligned}$$

There are no more free parameters. The next moment

$$\int_0^\infty x^2\,\mathcal{F}_2^{(4)}dx = -80/3$$

is reproduced in good approximation.

The representations (A25) and (A26) are excellent for our purposes, and can be safely used, reducing substantially the computation time.

APPENDIX B: INFLUENCE OF THE CONFINING AND NONCONFINING CORRELATORS ON HIGH-ENERGY SCATTERING

We have seen in Sec. II B that only one of the tensor structures present in Eq. (28) leads to confinement, namely the part of the correlator whose scalar function is denoted by D. If $\kappa = 1$ this is the only existing contribution, and since it has the property of leading to confinement, we refer to it as the *confining case*. The other tensor structure, which for $\kappa = 0$ is the only one contributing, is referred to as the *nonconfining case*. Comparing the effects of the two functions, we put

$$-\frac{1}{2}k^2\frac{d}{dk^2}\widetilde{D}_1(k^2) = \widetilde{D}(k^2) \qquad \text{(B1)}$$

in order to have the same spatial behavior for their contributions to the correlator.

In Fig. 16 we represent the reduced eikonal function $\widetilde{\chi}(\vec{b},\vec{R}(1,1),\vec{R}(2,1))$ for the case where $\vec{b},\vec{R}(1,1)$, and $\vec{R}(2,1)$ are all parallel and with a ratio $|\vec{R}|/a = 2$. The eikonal function $\widetilde{\chi}$ is plotted as a function of b/a, i.e., the impact parameter in units of the correlation length a. In the confining case the eikonal function is approximately proportional to the overlap region of the two loops in the transverse plane. In the nonconfining case there is a large contribution if both quarks or antiquarks from loop 1 and loop 2 coincide, i.e., for $b = 0$; the contribution is smaller if there is coincidence of only one particle (quark or antiquark) from of each loop. Thus in the confining case we have typically a true string-string interaction, while in the nonconfining case we have a quark-quark interaction.

In Fig. 17 we show the strong dependence of the eikonal function $\widetilde{\chi}$ on the orientation of the loops for the confining case. The figure shows $\widetilde{\chi}$ as a function of b/a, for the case that the loops are parallel in the transverse plane i.e., $\theta_1 = \theta_2 = \theta$. The common angle θ is a parameter, running from 0° to 80° in steps of 20°. In order to strengthen and make very visible the effect, we have cho-

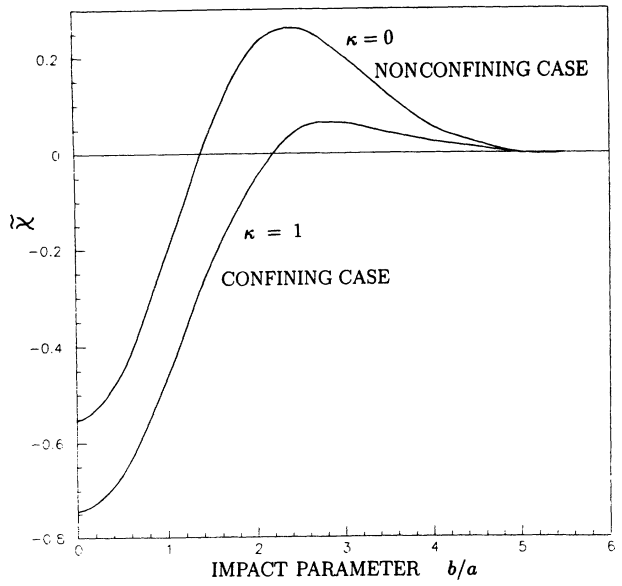

FIG. 16. Comparison of the values of the reduced eikonal functions $\widetilde{\chi}$ for the extreme pure confining ($\kappa = 1$) and pure nonconfining ($\kappa = 0$) cases, in a situation where the three vectors $\vec{b}$, $\vec{R}(1,1)$, and $\vec{R}(2,1)$ are parallel.

sen a large value $|\vec{R}|/a = 10$. From the figure we observe that the loops interact as one-dimensional objects in the transverse plane.

In Fig. 18 we show the cross section (in arbitrary units) as a function of the hadron extension S/a, using a Gaussian wave function $\sqrt{2/\pi}(1/S)\exp(-R^2/S^2)$. For $S/a \leq 1$, the two cases nearly coincide, but for larger values the cross section in the nonconfining case stays nearly constant, whereas the cross section for the confining case continues to increase approximately like $(S/a)^3$. Thus we have quark additivity only for the nonconfining case. Since the correlator for the confining case can only

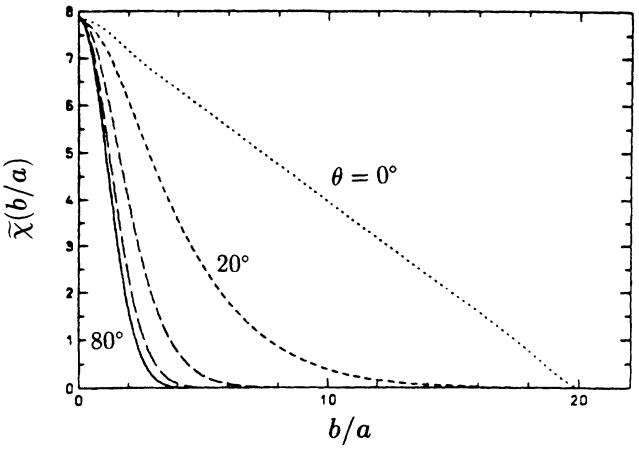

FIG. 17. Angular dependence of the reduced eikonal function $\widetilde{\chi}$ for the purely confining case ($\kappa = 1$). The figure shows results for configurations where the two interacting loops are parallel ($\theta_1 = \theta_2 = \theta$) and $|\vec{R}_1| = |\vec{R}_2| = 10a$. The angle θ varies from 0° to 80° in steps of 20°.

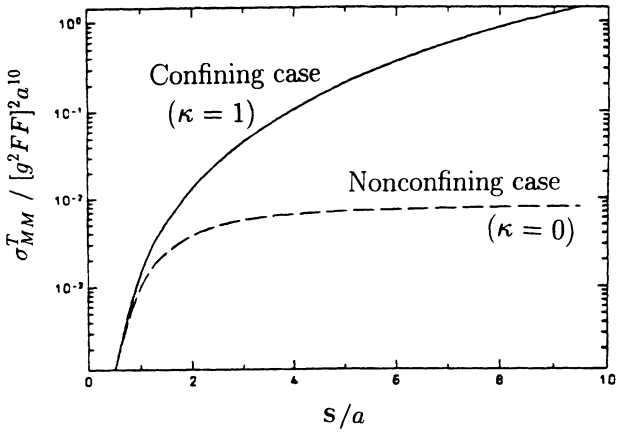

FIG. 18. Comparison of the total cross sections obtained in the two extreme conditions of $\kappa = 1$ (pure confining case) and $\kappa = 0$ (pure nonconfining case).

be present in a non-Abelian theory, an Abelian model will always yield quark additivity if $(S/a) \geq 1$ holds [16].

APPENDIX C: THE VALUE OF THE GLUON CONDENSATE $\langle g^2FF\rangle$

The most accurate determination of the gluon condensate $\langle g^2FF\rangle$ comes from sum rule analyses of the charmonium system. In their original paper on sum rules, Shifman, Vainshtein, and Zakharov [15] obtained the value

$$\langle g^2FF\rangle = 0.47 \text{ GeV}^4 . \tag{C1}$$

This analysis was extended [34], yielding, taken into account all observed ground states of given quantum numbers in the charmonium system the range of values

$$0.51 \text{ GeV}^4 \leq \langle g^2FF\rangle \leq 0.79 \text{ GeV}^4 . \tag{C2}$$

Other analyses [35–37] yield considerable higher bounds for the gluon condensate. The main uncertainties are [38] the error in the pole mass of the charmed quark, radiative corrections, and the contributions of higher condensates. The last point is the most difficult to control [36]. Models indicate that they could increase considerably the value of the gluon condensate [37,39]. A conservative estimate for the gluon condensate is

$$\langle g^2FF\rangle = (0.95 \pm 0.45) \text{ GeV}^4 . \tag{C3}$$

Novikov [40] has however argued convincingly against the larger values (say larger than 0.8 GeV^4) for the reason that the analyses yielding large upper bounds for the gluon condensate either rely on only one specific channel, or are based on particular models. A nondiagonal sum rule analysis of the matrix element $\langle 0|\widetilde{\mathbf{A}}_\mu|\pi\rangle$, with

$$\widetilde{\mathbf{A}}_\mu = \frac{1}{2} g\, \epsilon_{\rho\mu\alpha\beta}\, \bar{d}\, \gamma_\rho\, \mathbf{F}_{\alpha\beta}\, u , \tag{C4}$$

that is particularly sensitive to the gluon condensate, yields also a low value.

There is however another theoretical difficulty. In a world without light quarks the value of the gluon condensate could be considerably larger. A low-energy theorem has been derived [30] relating the change of the gluon condensate with respect to (light) quark masses with the quark condensate

$$\frac{d}{dm_q}\langle g^2 FF\rangle = \frac{96\pi^2}{\beta_1}\langle \bar{q}q\rangle \ , \qquad \text{(C5)}$$

where $\langle \bar{q}q\rangle$ is the light quark condensate and β_1 is the first coefficient of the Gell-Mann Low function. For SU(3) the factor is large, $96\pi^2/\beta_1 \approx 100$.

Since the quark condensate $\langle \bar{q}q\rangle$ is negative, an increase of the quark mass leads to an increase of the gluon condensate. In a world of pure gauge fields the gluon condensate would thus have a larger value. This *pure gauge* value is obtained from the *empiric* one, which refers to a world with three light flavors, by taking all masses to infinity, i.e., by integrating Eq. (C5) up to a value of m_q where the quarks decouple. The authors of the theorem [30] estimate that the pure gauge value is about two to three times higher than the empirical value. As argued in Sec. V, in our model we must use the pure gauge value of the gluon condensate.

[1] L.V. Gribov, E.M. Levin, and M.G. Ryskin, Phys. Rep. **100**, 1 (1983); E.M. Levin and M.G. Ryskin, *ibid.* **189**, 267 (1990); H. Cheng and T.T. Wu, *Expanding Protons: Scattering at High-Energies* (MIT Press, Cambridge, MA, 1987).

[2] CERN UA4 Collaboration, M. Bozzo *et al.*, Phys. Lett. **147B**, 392 (1984); CERN UA4/2 Collaboration, C. Augier *et al.*, *ibid.* B **316**, 448 (1993); Fermilab E710 Experiment, N.A. Amos *et al.*, Phys. Rev. Lett. **68**, 2433 (1992); Fermilab CDF Collaboration, F. Abe *et al.*, Fermilab Report No. Fermilab-Pub-93/232-E (unpublished); Fermilab Report No. Fermilab-Pub-93/234-E (unpublished).

[3] Data Compilations from Particle Data Group, K. Hikasa *et al.*, Review of Particle Properties, Phys. Rev. D **45**, S1 (1992); M.K. Carter, P.D.B. Collins, and M.R. Whalley, RAL Report No. RAL-86-002, 1986 (unpublished); review articles from L.L. Jenkovszky, Fort. Phys. **34**, 791 (1986); M.M. Block and R.N. Cahn, Rev. Mod. Phys. **57**, 563 (1985); some experimental data from D.S. Ayres *et al.*, Phys. Rev. D **15**, 3105 (1977); C.W. Akerlof *et al.*, *ibid.* **14**, 2864 (1976); S.F. Biagi *et al.*, Z. Phys. C **17**, 113 (1983); R. Majka *et al.*, Phys. Rev. Lett. **37**, 413 (1976); J.J. Blaising *et al.*, Phys. Lett. **58B**, 121 (1975); N. Amos *et al.*, *ibid.* **120B** 460 (1983); A. S. Carrol *et al.*, *ibid.* **61B**, 303 (1976); **80B**, 423 (1979).

[4] J.B. Burq *et al.*, Nucl. Phys. **B217**, 285 (1983).

[5] J. Badier *et al.*, Phys. Lett. **41B**, 387 (1972); S.F. Biagi *et al.*, Nucl. Phys. **B186**, 1 (1981).

[6] P.D.B. Collins, *An Introduction to Regge Theory and High Energy Physics* (Cambridge University Press, Cambridge, 1977).

[7] A. Donnachie and P.V. Landshoff, Phys. Lett. B **296**, 227 (1992).

[8] E.M. Levin and L.L. Frankfurt, Pis'ma Zh. Eksp. Teor. Fiz. **2**, 105 (1965) [JETP Lett. **2**, 65 (1965)]; H.J. Lipkin and F. Scheck, Phys. Rev. Lett. **16**, 71 (1966); H.J. Lipkin, *ibid.* **16**, 1015 (1966); J.J. Kokedee and L. Van Hove, Nuovo Cimento A **42**, 711 (1966).

[9] B. Povh and J. Hüfner, Phys. Rev. Lett. **58**, 1612 (1987); Phys. Lett. B **215**, 772 (1988); **245**, 653 (1990); Phys. Rev. D **46**, 990 (1992); C. Bourrely, J. Soffer, and T.T. Wu, Nucl. Phys. **B247**, 15 (1984); Phys. Rev. Lett. **54**, 757 (1985); Phys. Lett. B **196**, 237 (1987); J. Dias de Deus and P. Kroll, Nuovo Cimento A **37**, 67 (1977); Acta Phys. Pol. B **9**, 157 (1978); P. Kroll, Z. Phys. C **15**, 67 (1982); T.T. Chou and C.N. Yang, Phys. Rev. **170**, 1591 (1968); D **19**, 3268 (1979); Phys. Lett. 128B, 457 (1983); B **244**, 113 (1990).

[10] H.G. Dosch, Phys. Lett. B **190**, 177 (1987).

[11] H.G. Dosch and Yu.A. Simonov, Phys. Lett. B **205**, 339 (1988).

[12] D. Amati, S. Fubini, and A. Stanghelini, Nuovo Cimento **26**, 896 (1962).

[13] M. Gell-Mann, M.L. Goldberger, and F.E. Low, Rev. Mod. Phys. **36**, 640 (1964).

[14] F.E. Low, Phys. Rev. D **12**, 163 (1975); S. Nussinov, Phys. Rev. Lett. **34**, 1286 (1975).

[15] M.A. Shifman, A.I. Vainshtein, and V.I. Zakharov, Nucl. Phys. **B147**, 385 (1979); **B147**, 448 (1979); **B147**, 519 (1979).

[16] P.V. Landshoff and O. Nachtmann, Z. Phys. C **35**, 405 (1987); O. Nachtmann and A. Reiter, *ibid.* **24**, 283 (1984).

[17] A. Donnachie and P.V. Landshoff, Phys. Lett. B **185**, 403 (1987), **202**, 131 (1988); **207**, 319 (1988); Nucl. Phys. **B311**, 509 (1988); J.R. Cudell, A. Donnachie, and P. V. Landshoff, *ibid.* **B322**, 55 (1989).

[18] O. Nachtmann, Ann. Phys. **209**, 436 (1991).

[19] Y. Aharonov and D. Bohm, Phys. Rev. **115**, 485 (1959).

[20] N.G. van Kampen, Physica **74**, 215 (1974); **74**, 239 (1974); Phys. Rep. C **24**, 172 (1976); G.C. Hegerfeldt, and H. Schulze, J. Stat. Phys. **51**, 691 (1988).

[21] M. Schiestl and H.G. Dosch, Phys. Lett. B **209**, 85 (1988).

[22] Y.A. Simonov, Nucl. Phys. **B234**, 67 (1989).

[23] A. Di Giacomo and H. Panagopoulos, Phys. Lett. B **285**, 133 (1992).

[24] I.Ya. Arafieva, Theor. Mat. Fiz. **43**, 111 (1980); P.M. Fishbane, S. Gasiorowicz, and P. Kaus, Phys. Rev. D **24**, 2324 (1981); N.E. Bralic, *ibid.* **22**, 3090 (1980); L. Diosi, *ibid.* **10**, 2552 (1983); Yu.A. Simonov, Yad. Fiz. **48**, 1381 (1988); **50**, 213 (1988).

[25] A. Ringwald, Nucl. Phys. **B330**, 1 (1990).

[26] A. Krämer, Ph.D. thesis, Universität Heidelberg, 1991.

[27] A. Krämer and H.G. Dosch, Phys. Lett. B **252**, 669 (1990).

[28] A. Krämer and H.G. Dosch, Phys. Lett. B **272**, 114 (1991).

[29] H.G. Dosch, E. Ferreira, and A. Krämer, Phys. Lett. B **289**, 153 (1992).

[30] V.A. Novikov, M.A. Shifman, A.I. Vainshtein, and V.I. Zakharov, Nucl. Phys. **B191**, 301 (1981).

[31] Proton radius; G.G. Simon *et al.*, *Z. Naturforschung* **35A**, 1 (1980); pion radius, S.R. Amendolia *et al.*, Nucl. Phys. **B277**, 168 (1986); kaon radius, S.R. Amendolia *et*

al., Phys. Lett. B **178**, 435 (1986).

[32] C. Daum *et al., Proceedings of the E.P.S. International Conference on High Energy Physics, Geneva, 1979* (CERN, Geneva, 1979), Vol. 2, p. 628.

[33] T.T. Chou and C.N. Yang, Phys. Rev. **170**, 1591 (1968); A. Schiz *et al.*, Phys. Rev. D **24**, 26 (1981).

[34] L.J. Reinders, H. Rubinstein, and S. Yasaki, Phys. Rep. C **127**, 1 (1985), and references therein.

[35] R.A. Bertlmann, in *Non-Perturbative Methods*, edited by S. Narison (World Scientific, Singapore, 1986).

[36] J. Marrow, J. Parker, and G. Shaw, Z. Phys. C **37**, 103 (1987).

[37] B.V. Geshkenbein, Yad. Fiz. **51**, 1121 (1990) [Sov. J. Nucl. Phys. **51**, 719 (1990)].

[38] S. Narison, *QCD Spectral Sum Rules* (World Scientific, Singapore, 1986).

[39] H.G. Dosch and U. Lisenfeld, Phys. Lett. B **219**, 493 (1989).

[40] V.A. Novikov, M.A. Shifman, A.I. Vainshtein, and V.I. Zakharov, Nucl. Phys. **B237**, 525 (1984).